EXTENSION BETWEEN MAJOR FAULTS,

CENTRAL OREGON BASIN AND RANGE

by

ANUWAT TREEROTCHANANON

A THESIS

Presented to the Geological Sciences
and the Graduate School of the University of Oregon
in partial fulfillment of the requirements
for the degree of
Master of Science

September 2009

"Extension between Major Faults, Central Oregon Basin and Range," a thesis prepared by Anuwat Treerotchananon in partial fulfillment of the requirements for the Master of Science degree in the Department of Geological Sciences. This thesis has been approved and accepted by:

Dr. Ray J. Weldon II, Chair of the Examining Committee

Sept 4, 2009

Date

Committee in Charge: Dr. Ray Weldon, Chair
                            Dr. David Schmidt
                            Dr. Marli Miller

Accepted by:

Dean of the Graduate School

An Abstract of the Thesis of

Anuwat Treerotchananon   for the degree of   Master of Science

in the Department of Geological Sciences   to be taken   September 2009

Title: EXTENSION BETWEEN MAJOR FAULTS, CENTRAL OREGON BASIN

     AND RANGE

Approved: _____

                    Dr. Ray J. Weldon II

I present an alternative approach to determine the magnitude and direction of

extension in the Basin and Range Province at the north end of Summer Lake basin using

GIS techniques. Offset across 161 faults and tilting of 56 fault blocks were estimated to

calculate extension as a function of azimuth in this area. The orientation of a

representative set of slickenlines was collected in the field to assign average values for

the GIS analysis.

Azimuthal variation of extension is consistent with a strain ellipse indicating plane

strain with extension of 1.5 to 5.5 percent along the maximum extension direction of N75E

and no extension along the minimum N15W axis. Blocks tilt on average 60° from the

maximum extension direction, suggesting the underlying detachment dips ~N15E. This

technique allows strain associated with the numerous small faults to be added to the sparse

large faults for a complete regional analysis.

CURRICULUM VITAE

NAME OF AUTHOR: Anuwat Treerotchananon

PLACE OF BIRTH: Chiang Mai, Thailand

DATE OF BIRTH: August 28, 1979

GRADUATE AND UNDERGRADUATE SCHOOLS ATTENDED:

> University of Oregon
> Chiang Mai University

DEGREES AWARDED:

> Master of Science, Geological Sciences, 2009, University of Oregon
> Bachelor of Science in Geology, 2003, Chiang Mai University

AREAS OF SPECIAL INTEREST:

> Structural Geology

PROFESSIONAL EXPERIENCE:

> Geologist, Siam Minerals Commercial Co., Ltd., 2004
>
> Geologist, Petroleum Assessment Group, Bureau of Petroleum Technologies, Department of Mineral Fuels, 2003-2004
>
> Geologist, Environmental Geology and Geohazard Division, Department of Mineral Resources, 2003

GRANTS, AWARDS AND HONORS:

> Thai Government Science and Technology Scholarship, 2004

ACKNOWLEDGMENTS

TABLE OF CONTENTS

LIST OF FIGURES

Figure   Page

LIST OF TABLES

CHAPTER I

INTRODUCTION

The Basin and Range Province has been studied for decades. Elongated mountain ranges and parallel basins are the result of tectonic stretching of the earth crust, resulting in an increase in surface area. Its unique characteristics attracted many geologists to investigate it with a variety of approaches. Although the characteristics, mechanism and style of extension in the Basin and Range Province are known from these studies, some topics, such as the kinematics of variable fault orientations and block tilts are still controversial.

The Basin and Range Province, central Oregon, is surrounded by and includes many zones of active faults (Pezzopane and & Weldon, 1993; Weldon et al., 2003). Mapped patterns of normal fault linkages near Summer Lake show a systematic relationship between échelon step-sense, oblique-slip sense, and the position of linking faults (Crider, 2001). There has been long debate about the actual kinematics of fault displacement in this area of variable fault orientations and block tilts. The purpose of this study is to determine the magnitude and direction of extension in a particularly well exposed portion of the Central Oregon Basin and Range, and to develop a technique that can be efficiently applied to a large set of faults with a wide range of offsets and orientations. This will be accomplished by measuring the offset across faults and characterizing the tilting of fault blocks at the north end of Summer Lake Basin in south-

central Oregon using GIS techniques calibrated and tested by targeted field investigations. GIS allows the rapid characterization of a significant sample of the numerous, well-exposed faults in the area, and field investigations provide high quality data in selected regions to guide and validate the more extensive and easily generated GIS data set.

Location and Access

The Summer Lake basin is located in the northwestern corner of the Basin and Range Province in south-central Oregon at the center of Lake County. The study area is a region of extensional faulting (Donath, 1962; Donath & Kuo, 1962; Lawrence, 1976; Travis, 1977; Stewart, 1980; Zoback et.al., 1981; Pezzopane & Weldon, 1993; Crider, 2001; Badger & Watters, 2004) spanning approximately 385 km^2 between the north end of Summer Lake basin and the southern edge of Fort Rock Valley (Figure 1.1 and 1.2). The area appears on the bottom half of the Christmas Valley 30x60 minute quadrangle (1:100,000-scale) topographic map produced by the United States Geological Survey, 1986.

The region provides excellent exposure of block-faulted, gently-dipping Pliocene volcanic rocks that can be inferred to have been initially flat lying, and are essentially uneroded or buried subsequent to deformation (Figure 1.3). Thus it has attracted considerable attention (Donath, 1962; Donath & Kuo, 1962; Lawrence, 1976; Travis, 1977; Stewart, 1980; Pezzopane & Weldon, 1993; Crider & Pollard 1998; Crider, 2001; Badger & Watters, 2004) and offers a unique opportunity to apply GIS techniques to characterizing the deformation.
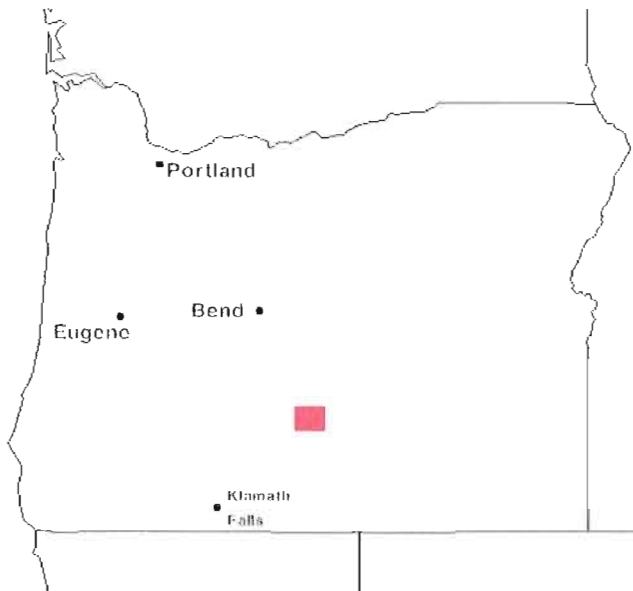
Figure 1.1. Map of Oregon showing location of Summer Lake area (red).

Figure 1.2. The location of the study area at the north end of Summer Lake basin. Dark lines are fault scarps and the intervening regions are tilted blocks of late Miocene to Pliocene largely basaltic volcanics.

Access is from Highway 31 that runs from U.S. Route 97 near the town of La

Pine (south of Bend, Figure 1.1) to Lakeview (east of Klamath Falls, Figure 1.1) along

western side of the study area. Good dirt and gravel roads such as County Highway 4-16

and Shuffield Road (Co Hwy 4-16A) only serve the northern part of Summer Lake

Valley. Fair to very poor gravel roads are used to access the hilly area beyond Summer

Lake Valley. Some sections of study area are difficult to reach due to inaccessible roads

and private landownership.

Figure 1.3. Exposure of a typical fault bounded tilt block, Klippel Point, in study area. The block dips gently west and has a steep east-facing escarpment. Photo looks north.

Geologic Setting and Background

Basin and Range structure of this region was first recognized by John Newberry

(1855) and was explored in 1870s-1890s by railroad companies and USGS geologists.

The study area is covered by a sequence of Tertiary volcanic rocks greater than 2000 m thick. The rocks are primarily basaltic and andesitic flows, interbedded with pyroclastic tuff and minor lacustrine sediments (Crider, 2001). Most of the area above the valley floor level is covered by the Pliocene Picture Rock Basalt (Travis, 1977) and older volcanics are only seen on the lower faces of fault scarps.

.   Regional fault structures show a broad range in strike, length, displacement, and degree of connectedness. Commonly the faults strike north-south, north-northwest, and north-northeast (Figure 1.2 and 1.4). Pezzopane and Weldon (1993) recognized the north-northwest striking faults are more numerous, generally shorter, and have less throw than those that strike north-northeast, which have greater throw along fewer yet longer faults. Fault throw is responsible for vertical relief in the region that ranges from a couple of meters to as many as several hundred meters. Winter Rim and Abert Rim are the largest structures in the region and show topographic relief of more than 750 m (Crider 2001).

The tectonic setting of the region is complex and has been interpreted in a variety of ways. Pease (1969) and Lawrence (1976) suggest that the orientation and offset of the N-NE-trending range bounding normal faults are controlled by northwest trending right-lateral faults. On the contrary, Donath (1962) described the structure in the Basin and Range Province in south-central Oregon. He claims that the structures in this area are influenced by several great north-south tectonic depressions that form a rhombic fault pattern in two principal sets -- N35 ºW and N20 ºE. Lawrence (1976) argued that the strike-slip movement along these two sets was prior to and contemporaneous with the generally later dip-slip deformation. Similarly, rhombic fault patterns in Basin and Range

province have been mentioned by many authors, included Piper, Robinson, and Park

(1939) in the Harney Basin of southeastern Oregon, and Allison (1949) in south-central

Oregon. On the other hand, Hamilton and Mayers (1966) state that the fault pattern

resulted from both right-lateral shear and extension. Likewise, Pezzopane and Weldon

(1993) hypothesize oblique rifting, based on the pattern of faulting as compared to known

oblique rifts.
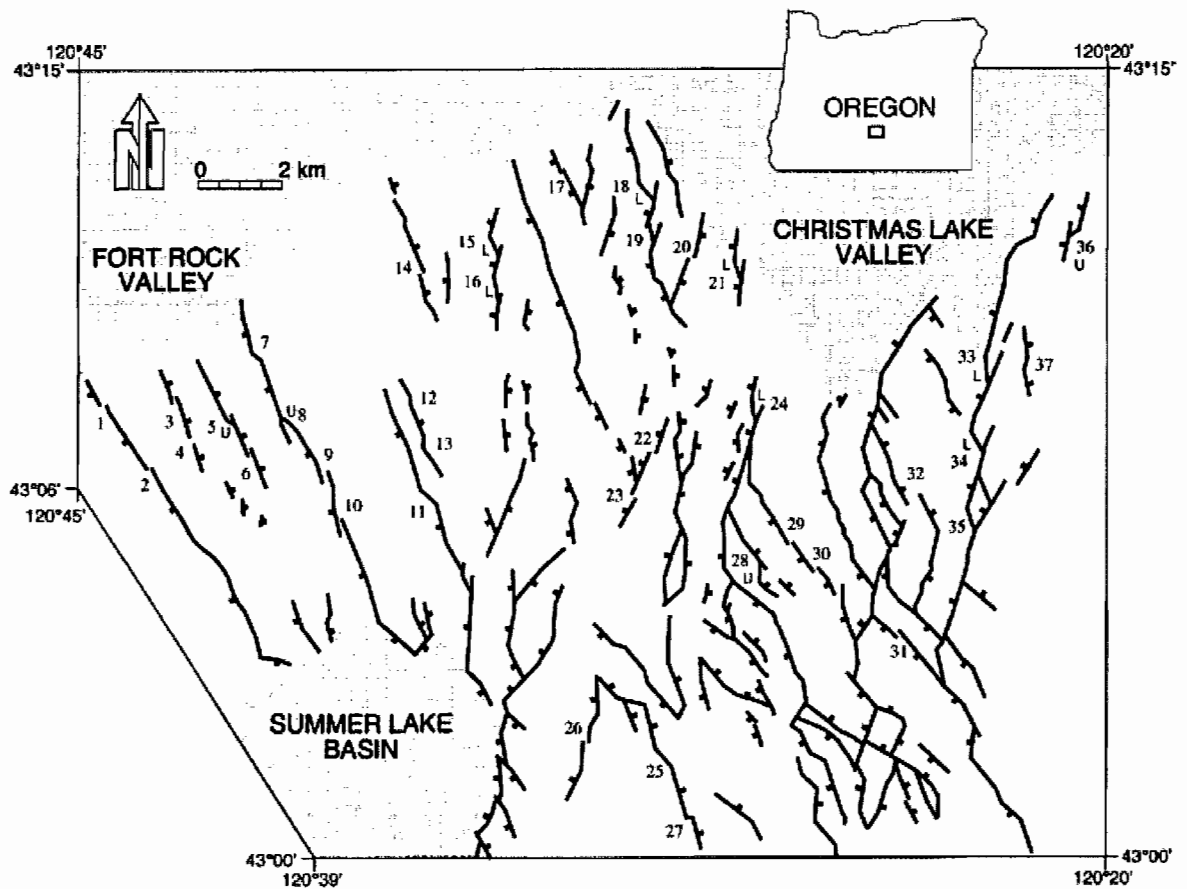
Figure 1.4. Simplified map of the fault pattern northeast of Summer Lake, Oregon. Faults are indicated by solid lines, tics on down-thrown side. (from Crider, 2001)

In addition to the fault orientations, the kinematics must explain the tilting of the blocks in between. Three basic models have been suggested to describe the Basin and Range structure: horst and graben, tilted block, and listric faulting (Figure 1.5). Stewart (1980) examined regional tilt patterns for major range blocks within the Basin and Range and Rio Grande Rift and identified broad regions of consistent tilt. His study reported that regional tilt domains are compatible with the tilted block model or the listric fault model but not the horst and graben model (Zoback et al., 1981). The study area also can be divided into regions with consistent tilts, suggesting variable dips on listric faults or the detachment surfaces underneath groups of similarly tilted blocks.

(a)

horst and graben

(b)

tilted block

(c)

detachment surface   listric fault

0   50 km
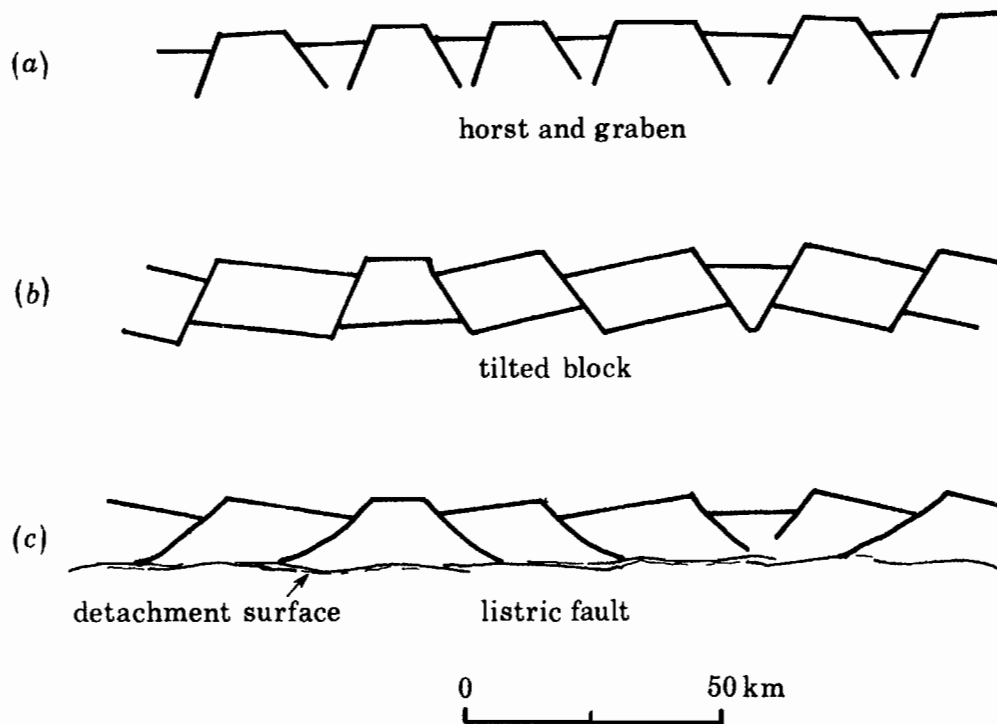
Figure 1.5. General models of basin and range structure. **(A)** Horst and graben model. **(B)** Tilted block model. **(C)** Listric fault model. (from Zoback et al., 1981)

Donath and Kuo (1962) ran a seismic-refraction profile along the northeast part of Summer Lake Valley in February, 1957 to determine whether the fault block structure underneath the large Quaternary basins is similar to that in the uplands area. The profile was run along an azimuth of N48 ° E, nearly perpendicular to the dominant structural trend. The interpretation from their study shows a complexly faulted lower layer oriented similarly to the upland. The dimensions of the fault blocks underneath are approximately 1800-2500 feet wide with a high velocity layer (interpreted to be volcanic unit) that varied from 300 feet to 1100 feet in depth. The dips of the inferred faults are very steep, dipping from 75° to 85° or greater. Vertical separations on the faults range from 200 feet to about 800 feet. In addition, they note that the surface faults observed in this area suggest that the majority of faults in the region may be vertical (Donath, 1962). Given the similarity of faulting in the exposed upland areas and that inferred below the basin, it can be concluded that the faulting in the upland area is also representative of the unexposed faulting beneath the basin.

The complex pattern of fault scarps in the uplands region is clearly identifiable on topographic maps and in aerial photographs. Interpretation of aerial photography indicates that this zone consists of numerous en échelon faults. The principle fault escarpments typically have zigzag and sharply curved traces, and appear geometrically segmented and separated. The Late Tertiary fault strikes in the Summer Lake area have been divided into two dominant trends which average about N35° ± 15°W and N25° ± 15°E (Pezzopane & Weldon, 1993). It is possible that the stress orientation could be changing and one trend cross cuts the earlier, although no author has published

compelling evidence of one trend consistently cutting the other. In fact, in many places, ramp and relay fault structures show a conjugate fault geometry with linked secondary splay faults, so both trends are seen in individual fault zones that appear to form and grow together. Such left-stepping, en échelon fault pairs are common in south-central Oregon, in zones that trend from northeast to northwest. These fault characteristics have been modeled to result from the sequential evolution of displacement, with continued extension across stepping echelon normal fault segments, the faults link to form continuous composite faults having zigzag traces (Crider, 2001).

The inferred regional horizontal extension direction is E-W to slightly ENE-WNW (Pezzopane & Weldon, 1993; Crider, 2001). Fault sets are oriented obliquely to extension direction. Since horizontal principal stresses (tensor components) are not perpendicular to the faults, the tectonics may be the result of extensional stresses oblique to fault strike, which in theory creates oblique rifting if every fault is individually consistent with the regional stress orientation. The theoretical consequence is that left-stepping faults that strike northeast have left-oblique normal displacement and right-stepping faults that strike northwest have right-oblique normal displacements, all within the same regional stress field.

Alternatively, the area could be expanding in all directions accommodated by the orthorhombic distribution of purely normal faults (Reches, 1978). In this case, all of the faults would be essentially normal and together they accommodate extensional strain oriented appropriately to the regional stress, although individual faults would appear to be inconsistent with the regional stress orientation. By measuring the slip directions on as

many faults as possible and attempting to add up all of the fault displacements and block tilts, I will calculate the real extension direction and magnitude, and determine which of these conceptual models best fits the data.

Basic Concept

This study investigates the magnitude of extension in all horizontal directions and combines them into a strain ellipse to determine the magnitude and direction of the net extension. Imagine that if we put a circle anywhere on the ground, before the region was deformed; after extension occurs the circle will become an ellipse (Figure 1.6).

Hans Cloos (1936) and his brother Ernst Cloos (1955) performed the simple clay deformation experiments by putting clay cake on top of an elastic rubber sheet and then stretching slowly and uniformly. The entire clay layer experiences the effects of the stretching. As a result, numerous closely spaced faults and fault scarps are developed (Figure 1.6). The clay cake shows lengthening in the direction of stretching, some fault traces are straight while others are curved, typically into high angle to the direction of extension (not clearly seen in the cartoon in Figure 1.6). Antithetic faults and a series of tilted fault blocks have been found similar to natural patterns in the study area. In order to get total extension, all extensions due to all faults as well as the area increased by tilted fault blocks have to be added up. With significantly large sample of faults and block tilts, the strain ellipse can be constructed.
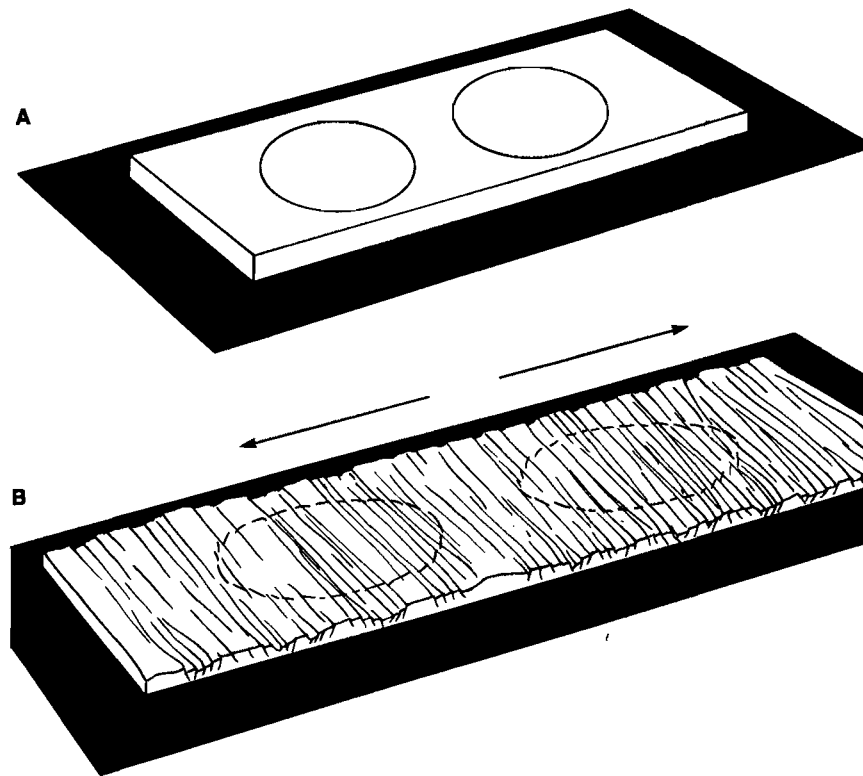
Figure 1.6. Clay cake experiment shows lengthening in the direction of stretching. **(A)** Clay cake on the rubber sheet. **(B)** After the rubber sheet has been stretched, the circles are deformed to an ellipse. (from Cloos, 1955)

It is assumed that all portions of the area under consideration experiences the same stretching. It does not matter what shape the area is. As long as a circle of the same size as the area being considered would catch the same number of faults, the location and the shape of the sampled area is not important. We can take any representative area or sum of areas of different shapes and calculate the size of a circle with the same area and catch the same amount of strain that a circle of that size would catch. As the area extends, the circle becomes an ellipse (Figure 1.7) that can be interpreted as a strain ellipse. The

maximum direction of the extension is the azimuth of the major axis of the ellipse. The minor axis will be the direction of least extension. If the minor axis is the same length as the radius of the initial circle (as shown in Figure 1.7), the region will have experienced no extension in that direction and thus we will have plane strain, i.e. vertical thinning = horizontal extension and no change in the 3rd dimension.

The area under consideration is called A_e, the expanded area. This is the representative area that has been stretched and can be measured on the map. All of the new area made is made by extension. The maximum direction of extension is the azimuth of the major axis of our ellipse. The original area, A_o, is the area of our initial undeformed hypothetical circle that will become the expanded ellipse.

The current area, the area of ellipse, is πab and the area of the original circle is πa^2. And if there is no extension in its short direction (as we will show below), a in the original circle equals a, the short axis in the ellipse. The expanded area minus the original area is the area added by extension. We called that "area added", A_a. We know the expanded area, A_e, because it is the area today, and we can calculate the area added, A_a, by adding up all of the area added by faults and block tilts. Using the difference between these we can solve for the original area, and then solve for the major (b) axis. If we know how long it is, we can calculate the percent strain using the formula;

$$A_e - A_o = A_a = \text{area added by extension}$$

$$= \pi ab - \pi a^2$$

$$A_a = \pi a(b - a) \quad \text{------------------} (1)$$

where a is the radius of original circle which we can find by taking area considered minus area added.

$$A_o = \pi a^2 = A_e - A_a \qquad \text{------------------ (2)}$$

$$\therefore a = \sqrt{\frac{A_e - A_a}{\pi}}$$

$$A_a = \pi a (b - a)$$

$$\frac{A_a}{\pi a} + a = b$$

$$\frac{A_a}{\pi a} = b - a$$

The difference between major and minor axis of the strain ellipse, b-a, is the area added

by extension divided by the radius of the original area times π, $\dfrac{A_a}{\pi a}$ and the length of b is

this value plus a.

To determine the total extension, we must add up the extension from each fault. The amount of extension depends upon 1) vertical separation across the fault, 2) the dip of the fault and 3) whether the dip changes with depth; i.e. whether the fault becomes listric. If the fault curves with depth, the extension approaches the displacement across the fault, rather than the horizontal component of slip for a planar fault (Figure 1.8). In theory one can relate the amount of curvature to the displacement and tilt of the hangingwall block, and I attempted to do this by characterizing the tilt of all of the blocks. However, we found that the tilt direction of the blocks was not in the same direction as the slip on the faults, so the problem is quite complex. Thus we decided to

bracket the extension by considering 2 end members, extension associated with all planar

faults and listric faults that curve to a horizontal dip (Figure 1.8). In other words, by using

the horizontal component of extension across each planar fault yields the minimum strain

and if we use the offset across the fault it will give us the maximum value (Figure 1.8).

We attempted to compare the amount of tilting of the blocks, estimated by tracing marker

beds within blocks or by calculating the surface slope of blocks, with the extension, as

will be discussed in detail below, but did not end up using it in the strain calculations.
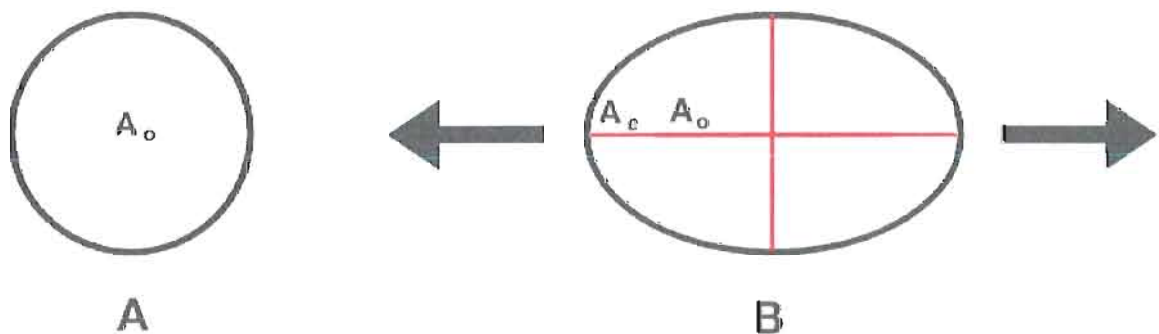
Figure 1.7. Geometry of strain ellipse under plane strain. **(A)** The area in circle
represents the original area. **(B)** After extension occurs, the circle will become an ellipse.

Extension Directions and Amounts

To determine the amount and direction of extension across each fault, the top and

the bottom of each fault scarp were digitized. Ideally, with planar layers and no

modification the vertical component of slip would be the height difference between the

top and bottom and the horizontal component would be the distance between the top and

the bottom of the scarp. However, since all fault scarps of the area have been modified by

collapse and erosion, top and bottom of scarps will have migrated back from the fault
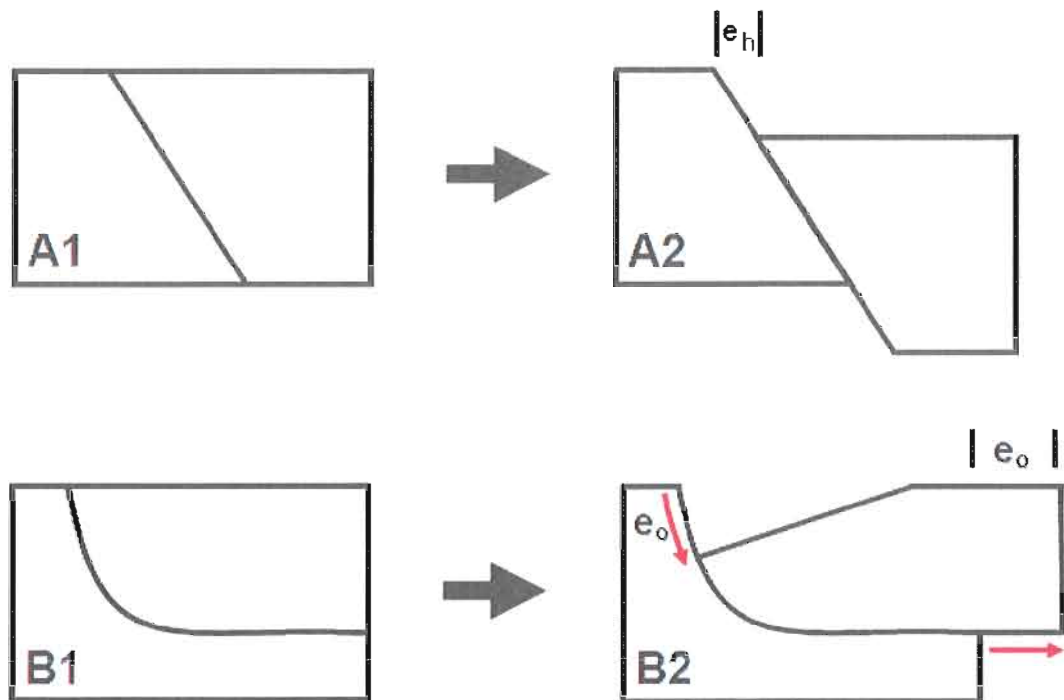
Figure 1.8. Schematic model shows an extension of each fault. **A)** With planar faults, extension is horizontal component of slip (e_h) on faults. **B)** With detachment faults, extension is equal to the offset (e_o) on faults.

(Figure 1.9) and the dip of fault must be known or inferred to calculate the true vertical and horizontal displacements. Since the dip of every fault cannot be observed, I collected a representative set of fault dips from the field to get an average value that was used to calculate the amount of extension for each fault (Figure 1.9). This field data will be discussed below in Chapter 3.
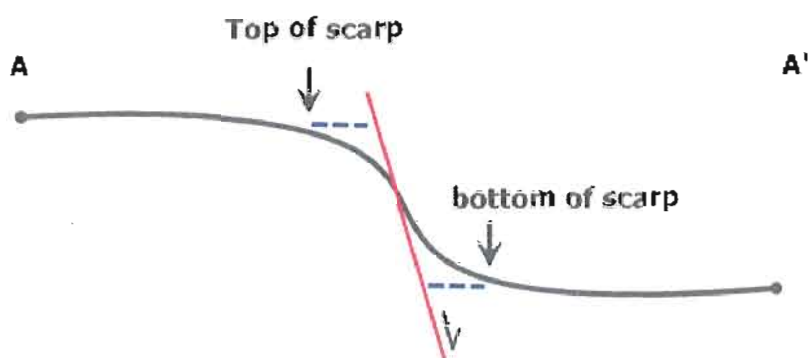
Figure 1.9. Simple cross section across a scarp. Top and bottom of fault scarp will be traced to get the extension.

In addition, we need to assign an extension direction for each fault or each fault segment, if we believe slip varies as the trend of the fault varies. As discussed in detail below in the results section, we found that slickenlines for all of the exposed fault planes record essentially pure dip slip motion regardless of their strike, so we assume that on average the slip direction is down dip for all of the faults. Thus the direction of extension is estimated by breaking the fault scarp into pieces (because the faults are not straight) and use the average dip of faults in the area to estimate amount of slip for each piece. We can determine how much slip occurs across each piece and infer whether the slip direction is perpendicular to that fault segment's strike. Each upper and lower fault trace was broken into 10 meter long sections and each section was converted into its central point (Figure 1.10). The nearest distance and direction between each top and bottom point is measured as well as the area, tilt direction and amount of tilt from each block, separated by the faults. From all of these pieces we make a histogram of the amount of extension as a function of direction, in 10 degree increments, by adding up all the different pieces for each direction. With these data we can calculate the strain and
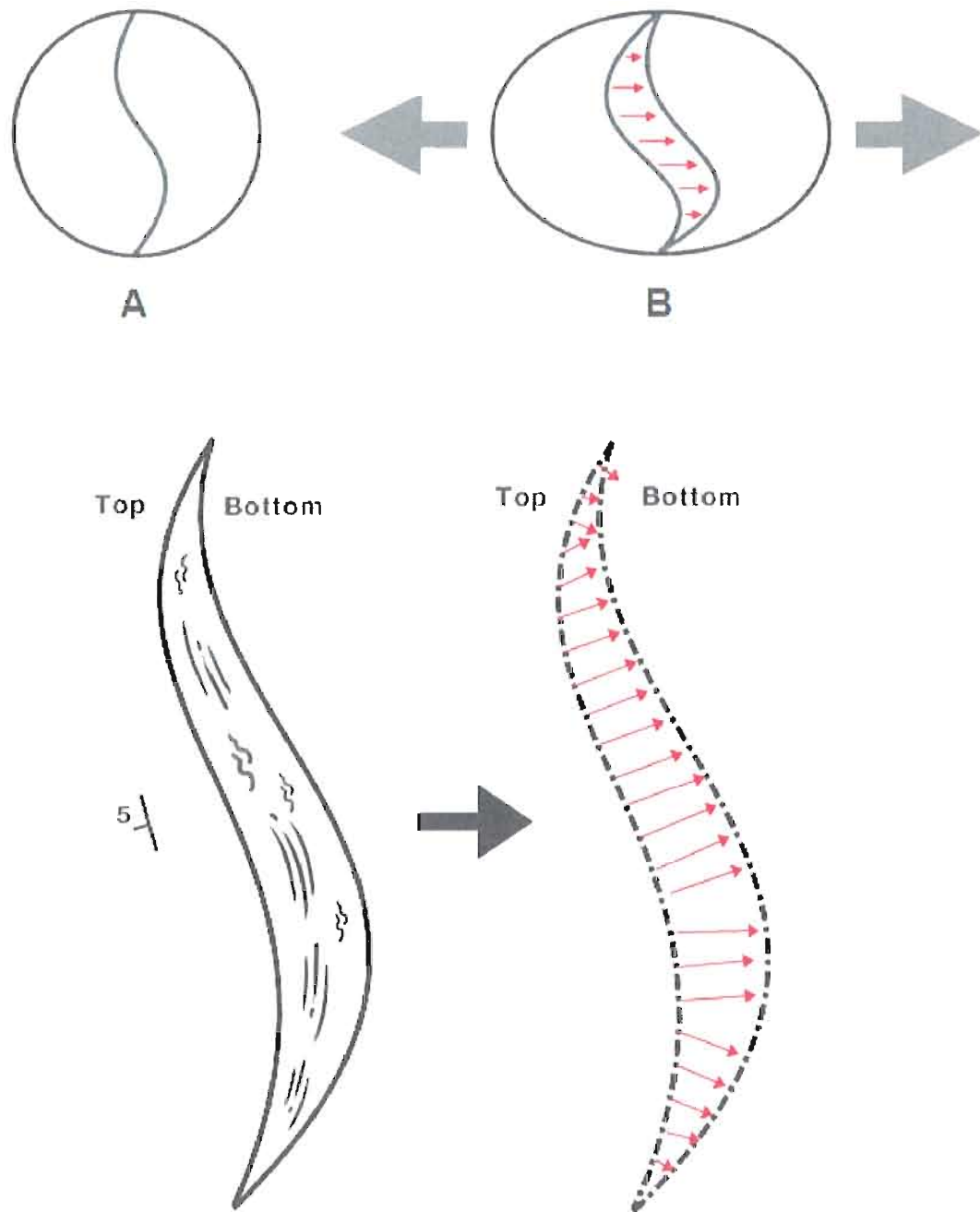
Figure 1.10. (Top) **A.** Closed crack in a circle. **B.** expanded crack making an ellipse under plane strain. (Bottom) Each fault scarp in the area is divided into 10-meter long pieces. The nearest top-bottom distance for each point is measured.

determine the direction of extension from the histogram as well as the magnitude of extension from added area occupied by faults and tilted blocks. The maximum value in the frequency distribution of the offset will show the direction of extension.

Although the magnitude and direction of extension can be estimated by adding up all extension, some extension is hiding in between the faults either by the tilting of blocks or other distributed deformation. Like the faults that we break into pieces, the size of the block is important because the same tilt of a big block contributes more extension than a small block.

Kautz and Sclater (1988) performed block faulting experiment using clay model, and compared their findings with the results from McClay and Ellis (1987) which were done on sand models. Their results suggest that 20-30% of the deformation was hidden or internal. So that when we add up the extensions due to the mapped faults we need to increase it by this amount to account to the small faults and the indiscernible internal strain. In our model, the hidden deformation might be small faults that are too small to map or small tilted blocks.

CHAPTER II

METHODOLOGY

In order to investigate the magnitude and direction of extension in the Basin and Range Province in central Oregon, 3D data is used to find block tilts and to completely determine slip across faults that vary in orientation and displacement along strike. This study used ESRI's geographic information system (GIS) software ArcGIS v.9.2. The USGS Digital Ortho Quad (DOQ) photography and Digital Elevation Model (DEM) were used as the base for identifying and mapping the faults and tilted fault blocks. The fault scarps were primarily drawn on overlays of the DOQ images and the layers of basalt flows (to determine tilt) were digitized from curvature maps generated from DEMs.

Data Collection and Map Construction

Digital elevation model (DEM) maps, developed from USGS 1/24,000 (7.5 minute) quadrangles provided by the U.S Geological Survey, have been used to interpret the geology in this study. These DEMs are created by interpolating the 10-foot elevation contours with a matrix of 10 meter grid spacing in latitude and longitude. In order to reconstruct bedding and fault orientation and to collect the data to determine fault offsets and tilt of block, the topographic surface is derived from the 10-m DEM obtained from GeoCommunity web site, freely available on the internet (http://data.geocomm.com /catalog/US/61056/429/group4-3.html). These DEMs are originally in the UTM NAD27

projection with vertical units in reference to National Geodetic Vertical Datum of 1929 (NGVD 29). In the UTM coordinate system, Earth is divided into sixty 6-degree-wide zones between 84 degrees N and 80 degrees S. North American Datum (NAD) 1927 or 1983 is used mostly for areas in North America as a reference system. However, the State Plane coordinate system can only be used within 50 states where states are divided into small zones based on political boundaries.

In order to overlay one or more layers from the same or different sources in ArcMap simultaneously, it is important to have all the data in the same coordinate system. For instance, a layer in State Plane coordinate system cannot be overlain with a layer in the UTM coordinate system. However, one can reproject the layer in State Plane into UTM coordinate system or UTM to State Plane system, since UTM is in metric system (in meters) and State Plane is in US metric system (in feet). The DEMs data of the study area are in UTM zone 10N that were reprojected to Oregon Lambert projection by The Oregon Geographic Information Council (OGIC)'s standard. The included DEMs are (see Figure 2.1 for their locations);

Saint Patrick Mountain, OR (43120a5)	Fandango Canyon, OR (43120b5)
Sheeplick Draw, OR (43120a6)	Christmas Valley, OR (43120b6)
Egli Rim, OR (43120a7)	Thorn Lake, OR (43120b7)
Duncan Reservoir, OR (43120a8)	Tuff Butte, OR (43120b8)

The Digital Ortho Quads (DOQs) are in MrSID format and can be found at Oregon Geospatial Enterprise office (GEO) web site at http://www.gis.state.or.us/data/

DOQ2000DL.html. These photos were taken in the year 2000, and are black and white with approximately one meter resolution. All DOQ photos can be found on the GEO web site except the photo 43120b7 that was obtained from http://www.reo.gov/dem/ore/ in TIF format. The referenced image was fixed to an Earth coordinate system, which was described by datum and projection (in this project North American 1983 HARN and Oregon Statewide Lambert). The georeferencing of the images, in MrSid format, has been done using ground control points, referenced from the already georeferenced DEM and the .sid and the .sdw files from MrSID packages data.

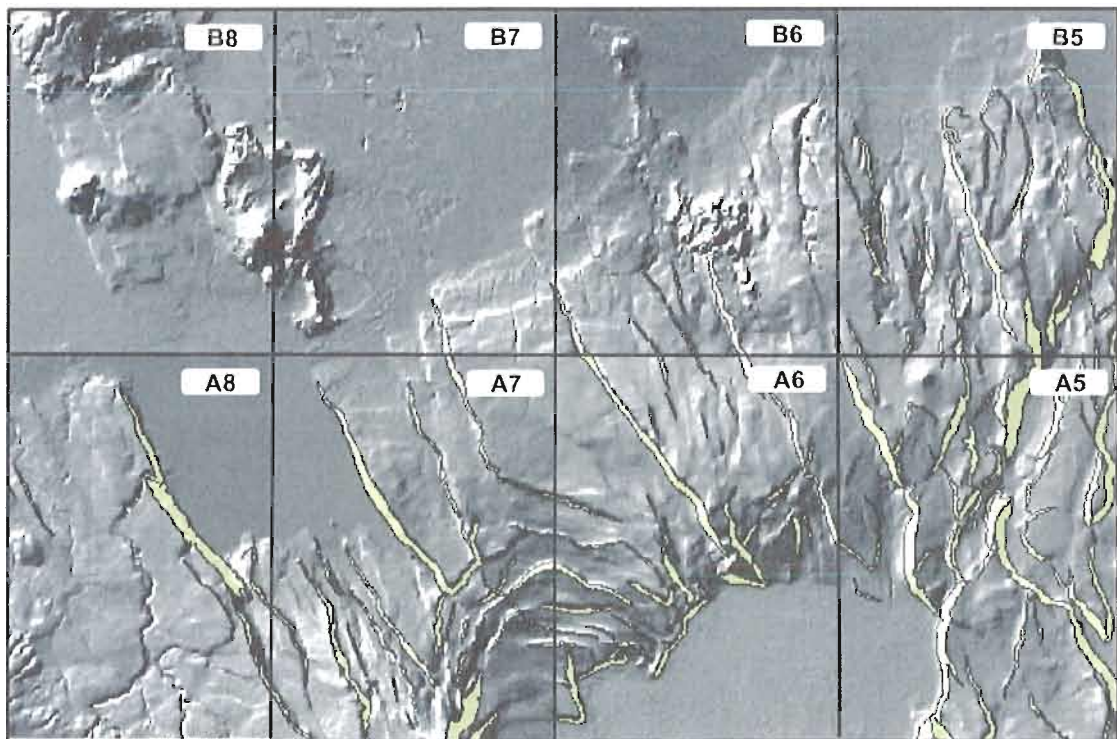**Figure 2.1.** Index of DEMs. **(A5)** Saint Patrick Mountain, OR (43120a5). **(B5)** Fandango Canyon, OR **(43120b5). (A6)** Sheeplick Draw, OR (43120a6). **(B6)** Christmas Valley, OR **(43120b6). (A7)** Egli Rim, OR (43120a7). **(B7)** Thorn Lake, OR **(43120b7). (A8)** Duncan Reservoir, OR (43120a8). **(B8)** Tuff Butte, OR (43120b8). Top-bottom boundaries of fault scarps are shown in yellow.

The output of the curvature function is the second derivative of the topographic surface (i.e., the slope of the slope). The curvature function will calculate the curvature of a surface at each cell center. A positive curvature indicates that the surface is upwardly convex at that cell. A negative curvature indicates that the surface is upwardly concave at that cell. A value of zero indicates that the surface is flat (ESRI, 2007). The curvature function allows us to easily recognize and digitize beds of basalt flows along the continuous convex and concave lines.

Reprojecting and Combining the Layers

The coordinate system of the DOQ photos (HARN Oregon Statewide Lambert Feet International and in North American Datum 1983) are reprojected into HARN Oregon Statewide Lambert (metric system) by using the "*Project*" tool under the projection and transformation toolset in the *Data management* toolbox.

In the *Project* dialogue box, click the first icon to put the data which we wanted to reproject then clicking the second icon to select the output location of reprojected data. Finally, we selected the coordinate system in which the data is reprojected by clicking the icon. All the coordinate and projection information of shapefile are stored in text file with .prj extension (Figure 2.2).
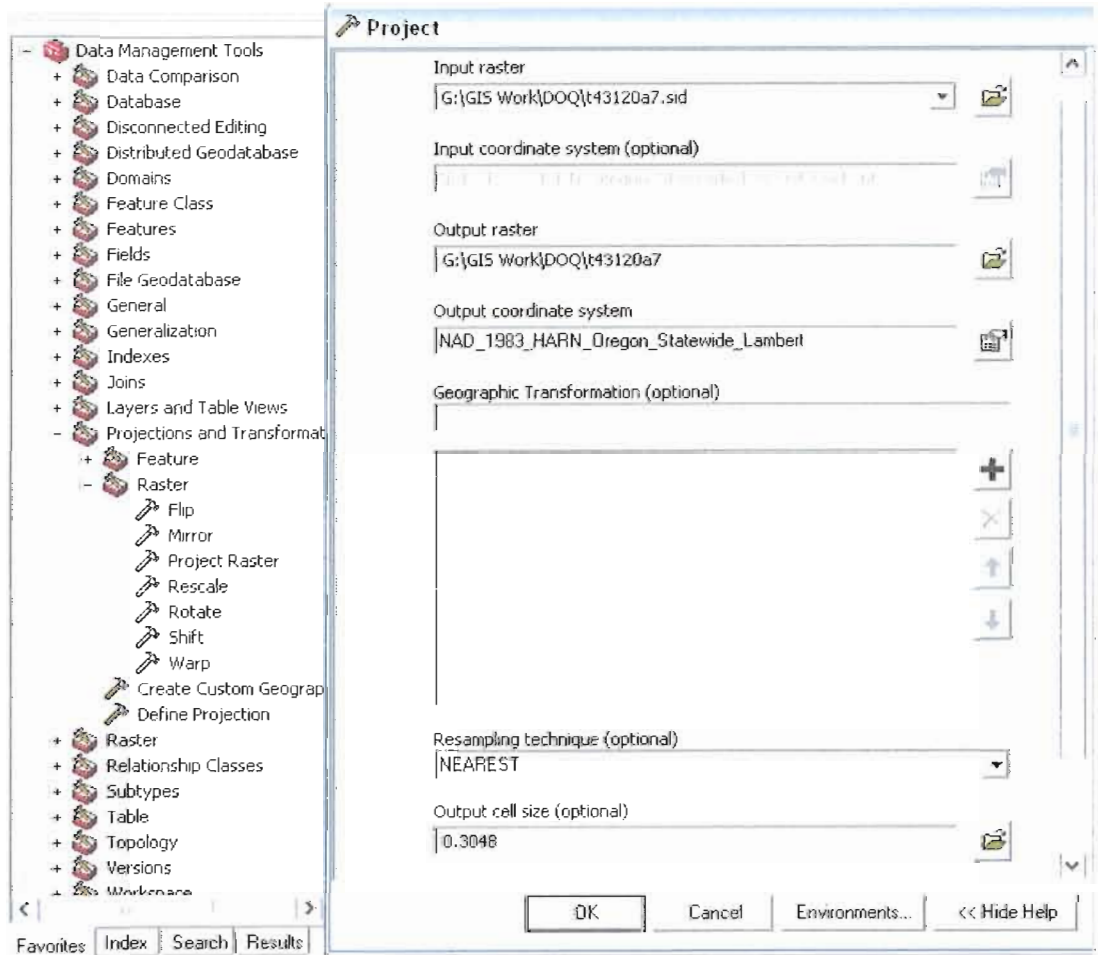
Figure 2.2. Selection of tool and toolset in *Data management* toolbox and dialogue box for reprojection of layers.
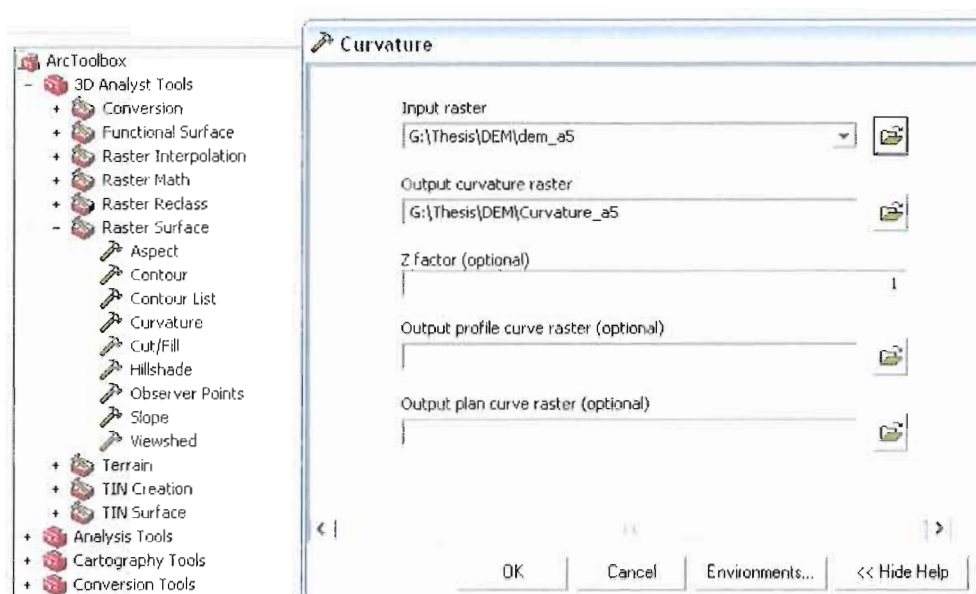
Figure 2.3. Selection of tool and toolset in *3D Analyst* toolbox and dialogue box to create curvature maps.

Creating 3D Curvature Maps

To create the curvature map in *ArcToolbox* at the *3D Analyst* tools, select the curvature in raster surface. In the *curvature* dialogue box, click the first ⬜ icon to put the raster data (DEM) from which we want to create the curvature and then click the second ⬜ icon to select the output location of data. Finally, selected the Z factor = 1 (Figure 2.3).

Traced Beds and the Top and Bottom of Fault Scarps

From the curvature map, now we can see the top and bottoms of the fault scarps and the layers of lava flows outcropping within them (Figure 2.5). The next step is digitizing the layers of lava flows to get the tilt of blocks and the top/bottom of the fault scarps to calculate offset and extension. A blank shapefile was first created in ArcCatalog

before digitizing a feature. This is done in ArcCatalog by right clicking and selecting

New >> Shapefile, filling in an appropriate name, setting the feature type to "polyline",

editing the coordinate system to UTM NAD83 Harn Oregon Statewide Lambert, and then

adding the new shapefile to ArcMap (Figure 2.4). Layers of lava flows were digitized

from the curvature map to calculate their inclination of the tilting fault block (Figure 2.6)

comparing with the tilting obtained from surface slope which is easier to measure.

Results from these two methods are compared in discussion chapter (Chapter 3, Table 2).

Figure 2.4. Creating the new shapefile in ArcCatalog. Right click and select *New >> Shapefile*.

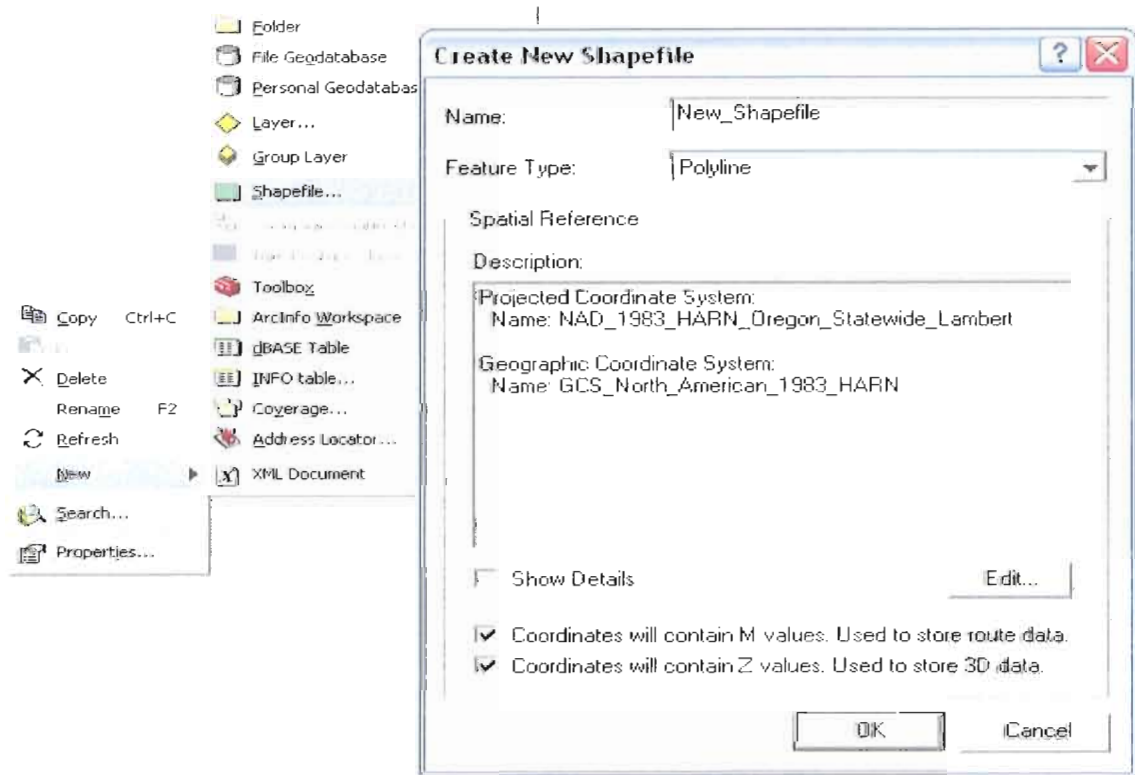The top and bottom of fault scarps as well as the boundary of the tilted fault blocks in the area of interest were digitized in the same manner as the layers of lava flows. But instead of setting the feature type when creating the new shapefile to polyline for the layers, change the feature type to "polygon" for top and bottom of the fault scarps. This will allow us to calculate the area added, the expanded area occupied by faults and tilted fault blocks (Figure 2.7).

Breaking Faults into Pieces and Relating Points on Top and Bottom of Scarps

Top and bottom boundaries of fault scarps were broken into pieces, to capture the variability in trend and displacement along the faults. This process divides and creates a reference point at 10 meters spacing for each fault trace. Top and bottom traced lines must be in the same convention, i.e. north to south and west to east in this study. In case that a line is not in that convention, it can be flipped by selecting "*Modified task*" in "*Edit Editor*" toolbar and right click to get into the "*Flip*" menu. Each top and bottom line were exported to a new file from selection tool and divided into 10 m pieces using "*Divide*" tool in Edit Editor toolbar. These reference points will be saved from start to end point ordered in our target point feature file. At this time, the reference points are only points along the line without xyz coordinates. So we need to assign them coordinates by using "*Data Management Tools >> Features >> Add xy coordinates*" for xy coordinates and "*Spatial Analyst Tools >> Extraction >> Extract Values to Points*" for z value.

27
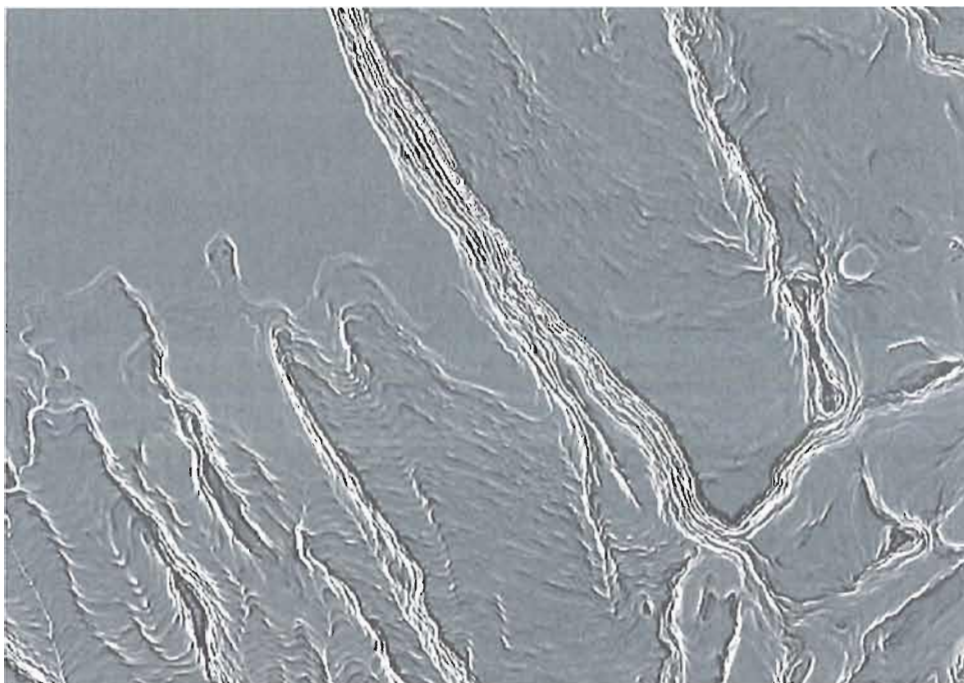
Figure 2.5. The curvature map in the southwest part of the study area shows the layers of lava flows exposed on fault scarps.
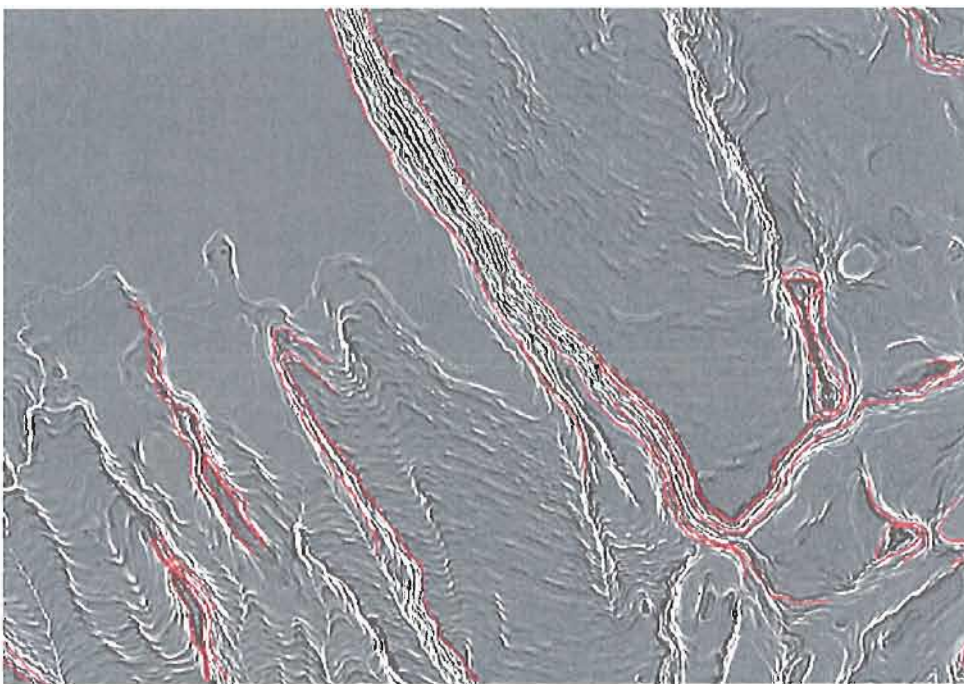
Figure 2.6. The layers of lava flows (red) were digitized from the curvature map.
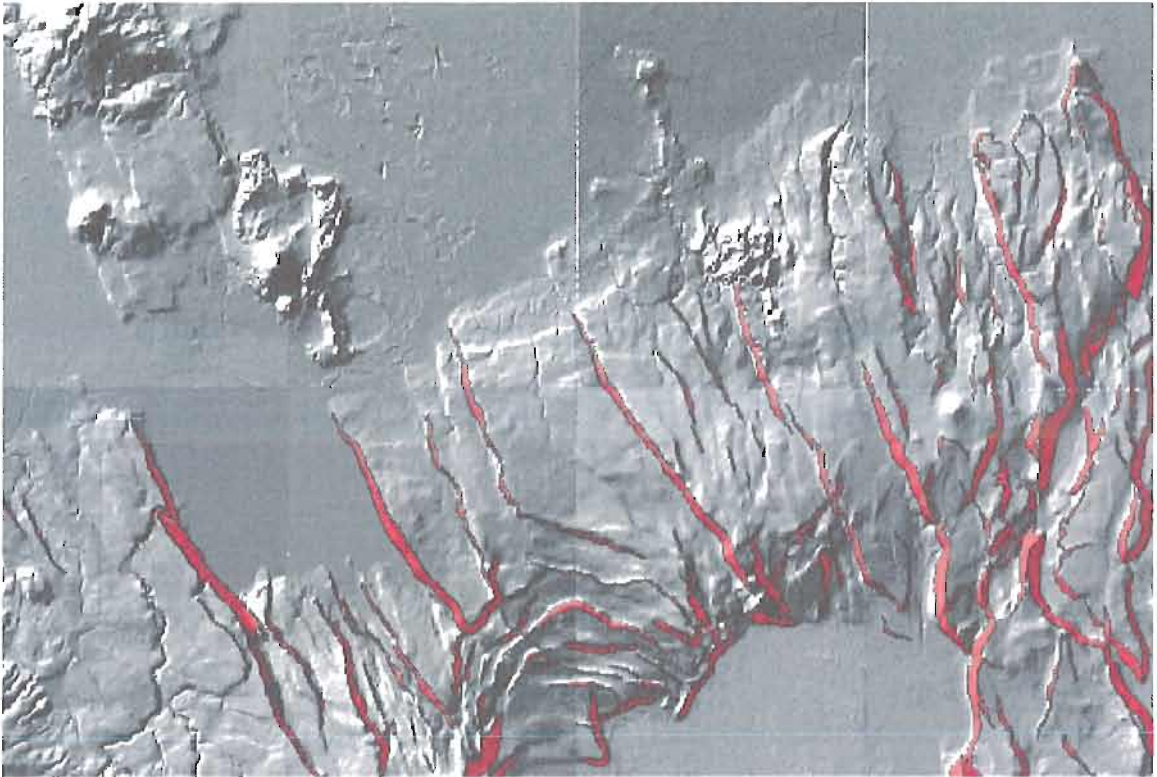
Figure 2.7. Fault scarps, red on hillshade image, are digitized in polygons to calculate expanded area generated by faulting.

Each reference point on the upper line was used to find the nearest point on the lower line to estimate amount of slip and direction of extension (Figure 2.8) by using "*Analysis Tools >> Proximity >> Near*" in *ArcToolbox*. In the dialog, put the top scarps in 'Input Features' and bottom scarp in 'Near Features'. Also, the search radius needs to be adjusted to an appropriate value for each fault.
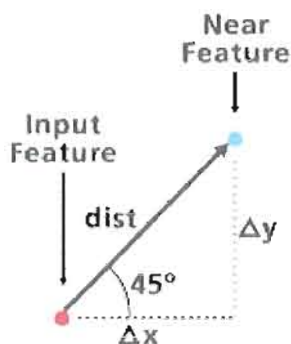
Figure 2.8. Diagram shows nearest point in *Nearest point analysis*. (Figure from ESRI, 2007).

Angles from '*Near*' analysis are measured in degrees, where one degree

represents 1/360 of a circle, and fractions of a degree are represented as decimal points.

Angles are measured from 180° to -180° ; 0° to the east, 90° to the north, 180° (-180°) to

the west, and -90° to the south (Figure 2.9).
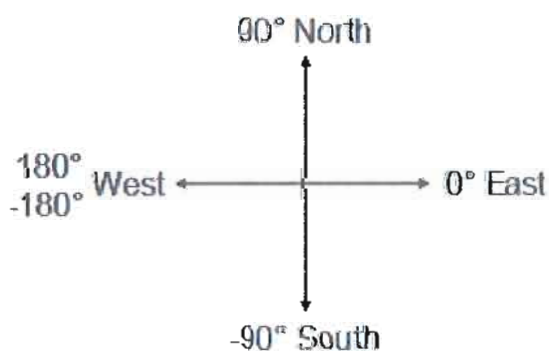
Figure 2.9. Angle convention from nearest point analysis. Angles are measured from 180° (anticlockwise) to -180° (clockwise) from east.

In order to convert to azimuth, following VB script is applied in the *calculate* tool;

```
Dim newAngle As Double
newAngle = [NEAR_ANGLE] + 270
While newAngle > 360
        newAngle = newAngle - 360
Wend
newAngle = 360 – newAngle
```

where [NEAR_ANGLE] is the name of the field in attribute table from '*Near*' analysis result.

Finally, join the calculated result together. In the dialogue, choose "Join data from another layer based on spatial location" and then join the upper and lower faults' attribute tables.

Determining Area, Tilt Direction and Amount of Tilt from Each Block

Fitting a Best-Fit Plane to 3D Georeferenced Data

This procedure allows the calculation of the strike and dip of any surface or bed for which you have a set of 3D georeferenced data points defining that surface. I start by calculating the best-fitting plane for the selected points, and then calculating the slope and aspect of this plane. We can also evaluate the quality of the fit for the plane through an output of the Root Mean Squared (RMS) error value.

To calculate the best-fitting plane for the selected points, I individually add the shapefiles of selected point data for each basalt flow bed. We then calculate the best-

fitting plane by selecting "*Raster Interpolation >> Trend*" command under *3D Analyst Tools* (Figure 2.10).
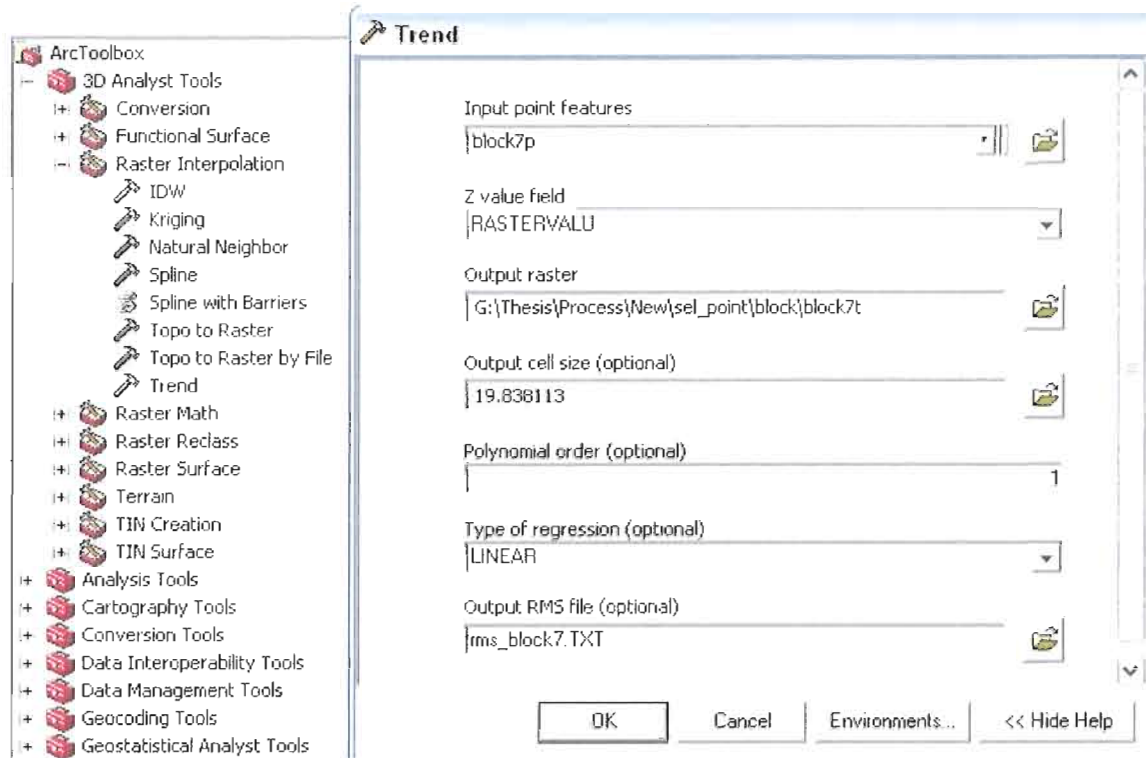
Figure 2.10. Trend dialogue in 3D Analyst Tools box.

In the *Trend* dialogue;

    a. "Input point feature" – select the shapefile from the pull-down menu

    b. "Z value field" – select the field containing Z values from the pull-down menu (if it is a shapefile enabled to store Z value, the "shape" option on the pulldown menu should work too).

    c. "Output raster" – browse to where you want the file saved and give the file a name.

    d. "Output cell size" – the default size should be fine.

    e. "Polynomial order" – should be 1.

    f. "Type of regression" – keep as 'Linear'.

    g. "Output RMS file" – browse to a location and name the file to save a text file of the coefficients for the plane equation, RMS error value, and a Chi-squared value.

And then click OK, the best-fit plane will plot under selected point on ArcMap (Figure 2.11).

To determine the dip of the plane:

In *ArcToolbox*, under *3D Analyst >> Raster Surface*, select *Slope* (Figure 2.12).

In this dialogue:

    1. "Input raster" – select your plane.

    2. "Output raster" – select a name and location for your slope map.

    3. "Output Measurement" – make sure this is 'Degrees'

    4. Then click OK.

This will assign colors based on the value of the dip. There may be a fringe of lower dip values on the edges of the plane, but by using the *Identify tool* and clicking in the center of the plane, the software will tell you the appropriate dip value (Figure 2.13).
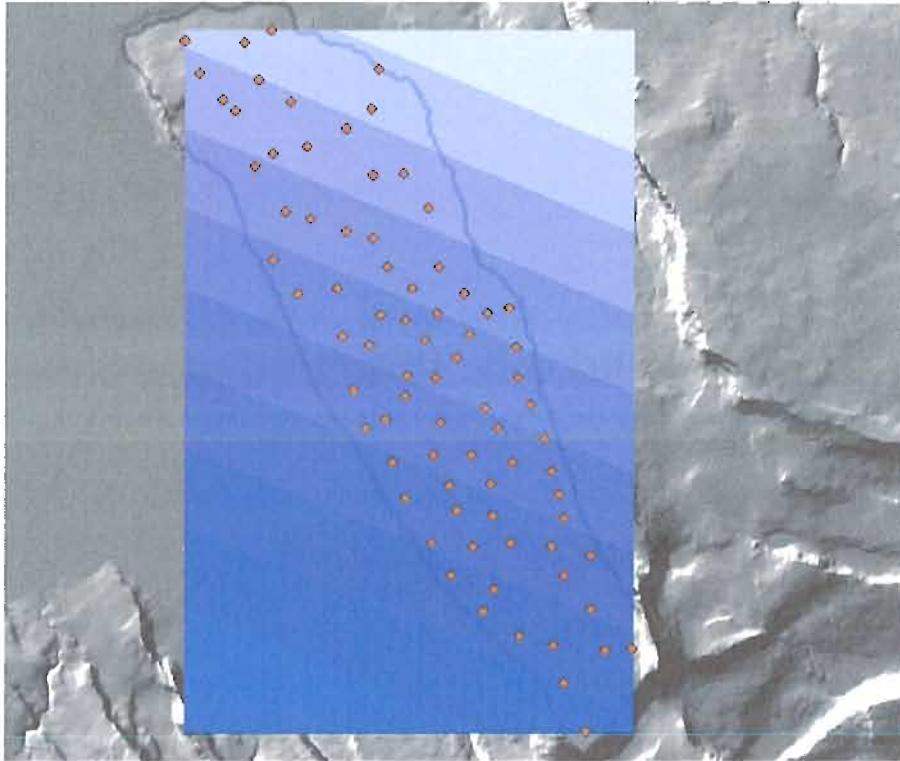
Figure 2.11. Elevation trend of selected surface. Color scale showing elevation trend of the surface from high (dark blue) to low (pale blue).

To determine the strike of this plane:

In *ArcToolbox*, under *3D Analyst >> Raster Surface*, select *Aspect*.

In this dialogue:

1. "Input raster" – select plane

2. "Output raster" – select a name and location for your aspect map.

3. Click OK.

This will assign colors based on the direction the surface is facing, which equals the dip direction. Click on the plane with the *Identify tool* to obtain the dip direction value, and subtract 90 degrees from this to convert into the strike (Figure 2.14).
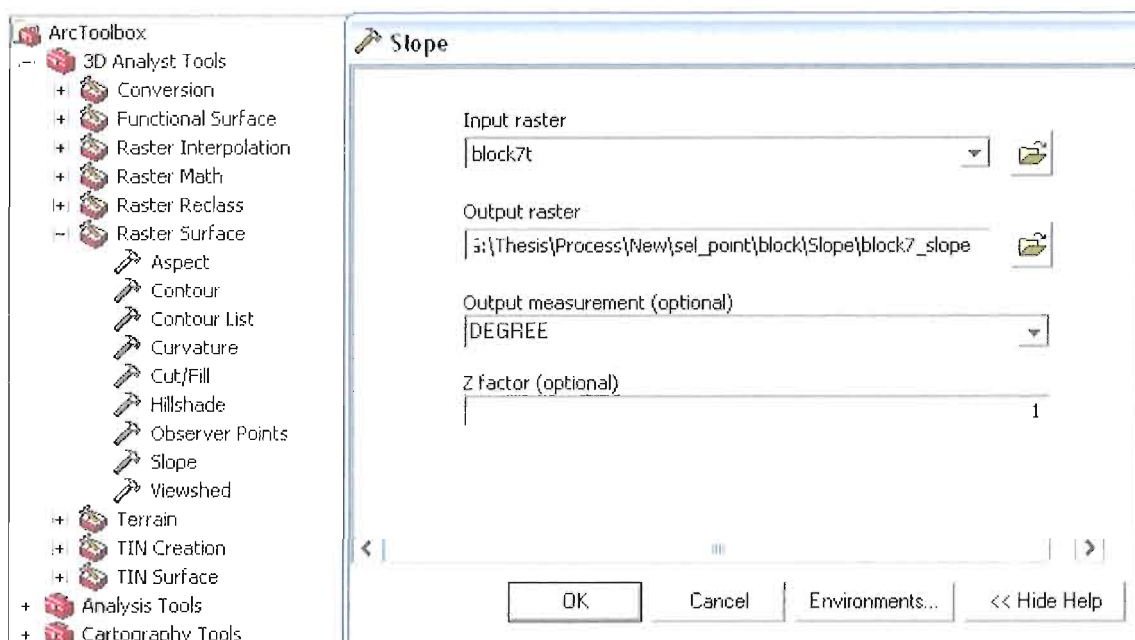
Figure 2.12. *Slope* dialogue and parameter in *3D Analyst Tools* box.
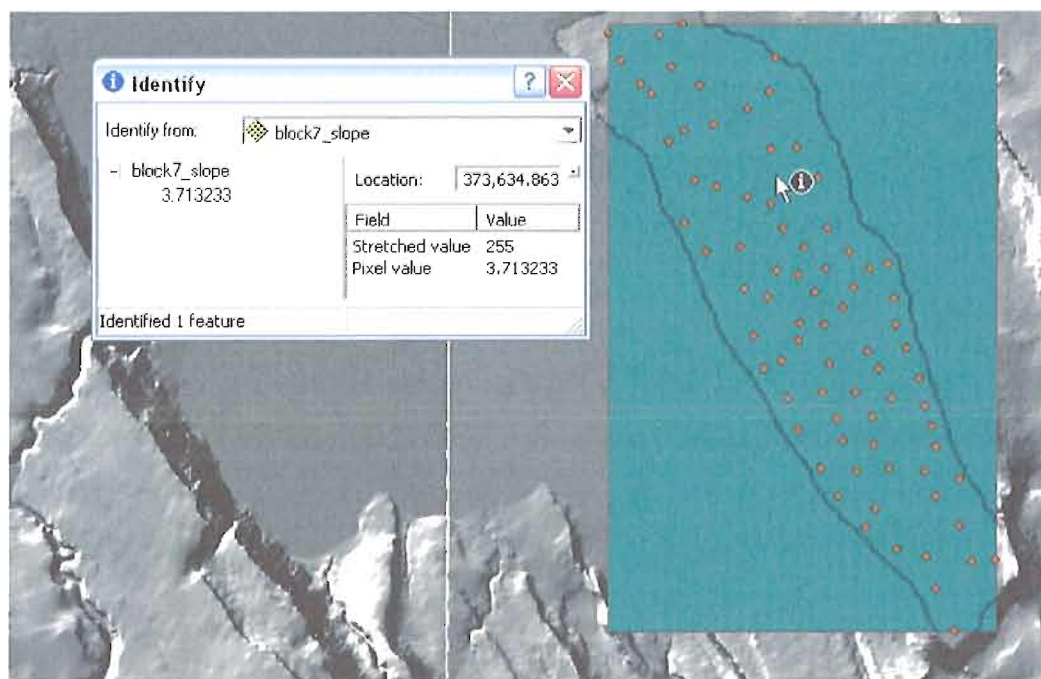
Figure 2.13. *Identify cursor tool* showing surface slope of selected area.
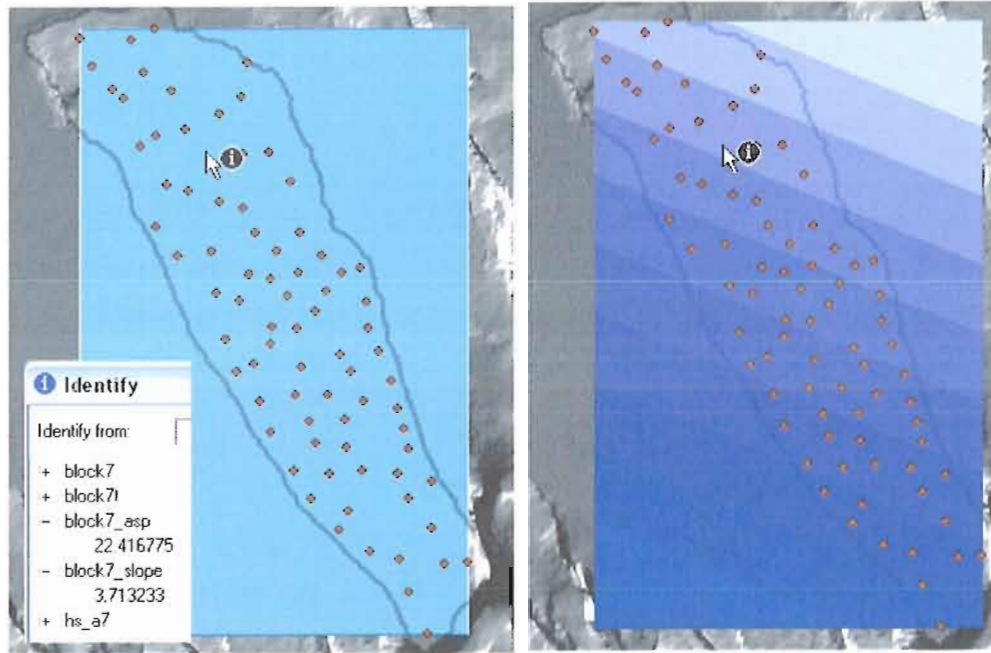
Figure 2.14. Result from '*Trend*' command or best-fit plane (right) comparing with calculated aspect (left). Strike of the surface is equal to aspect subtracted from 90. Left figure showing aspect of 022 or strike of 068, perpendicular to elevation trend.

CHAPTER III

RESULT AND DISCUSSION

161 fault scarps and 56 fault blocks at the north end of Summer Lake Basin were analyzed using GIS techniques and targeted field investigation (Figure 3.1). Faults forming a set with a primary trend of 330° and a secondary trend of 025°, separated by an angle of 55°, are commonly observed in the study area (Donath, 1962) (Figure 3.2). Five of the faults are over 1 kilometer long and approximately 130 escarpments are shorter than 500 meters. The area directly north of Summer Lake Valley is structurally uniform with faults trending about N30°W while the area north-northeast of Summer Lake Valley is more complex with less prominent faults, including a concentric and radial set (Travis, 1977). The vertical component of the displacement (ΔZ) ranges from 202 to 5 meters with an average of 36 meters. Horizontal component ranges from 56 to 1 meter with an average of 10 meters. Fault blocks generally tilt a few degrees.

The results from the nearest point analysis, Figure 3.3, show the orientation of all of the inferred displacement vectors. The directions (which are perpendicular to the fault strike in each 10 meter piece of a fault) and directional scatter are similar to earlier studies (e.g. Figure 3.2). The northwest-trending set is dominant in Summer Lake area, consistent with previous studies (Donath, 1962; Pezzopane & Weldon, 1993).
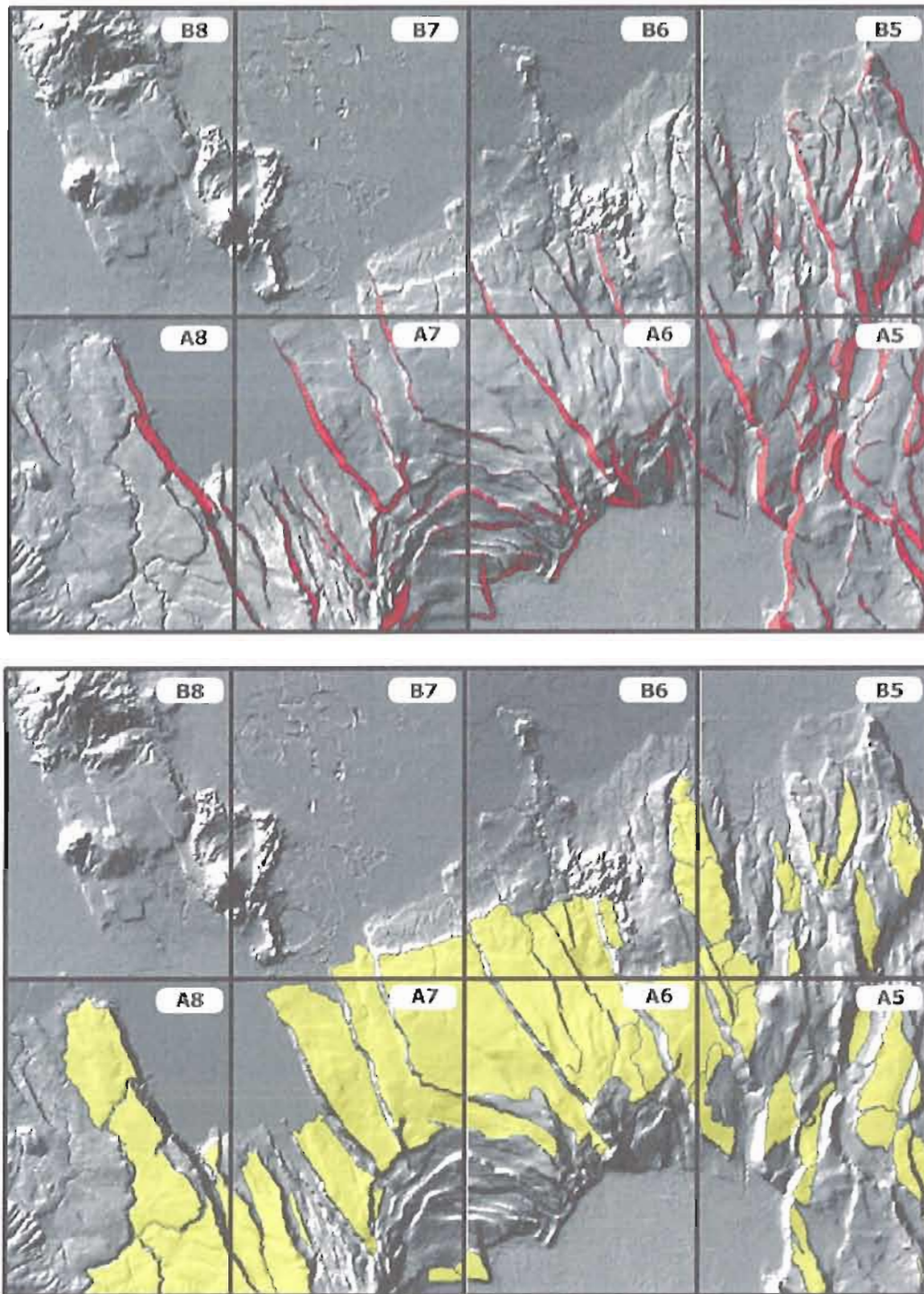
Figure 3.1. 161 fault scarps (upper) and 56 fault blocks (lower) at the north end of Summer Lake Basin.
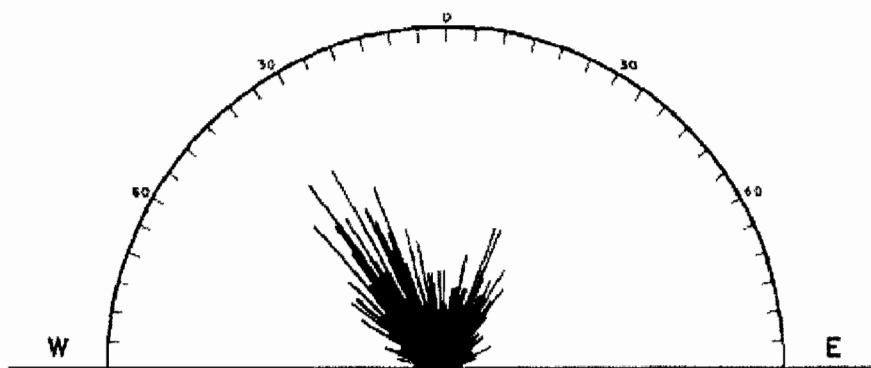
Figure 3.2. 625 faults and fault segments plotted at 1° intervals. Radius of diagram equals 18 faults or fault segments. A conjugate fault set of primary trending 330° and secondary trending 025°. (from Donath, 1962)
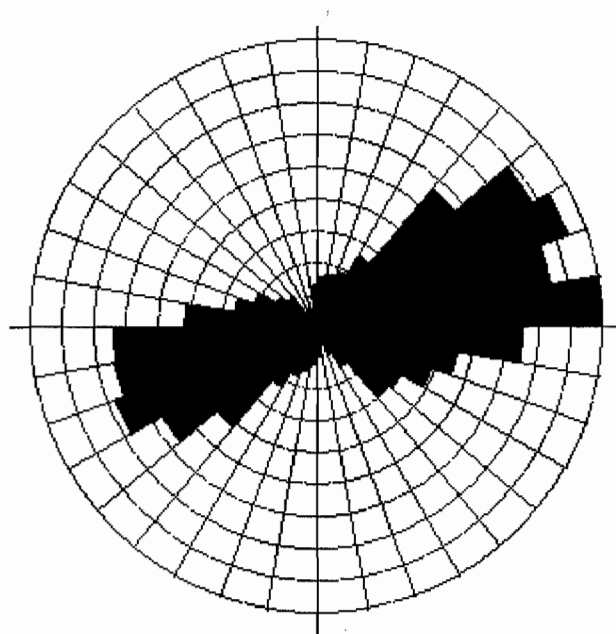
Figure 3.3. Rose diagram from near point analysis illustrates ENE-WSW azimuthal distribution of the offset vectors. Each bin is proportional to the number of fault scarps. Strike approximately normal to offset vector.

Due to the limitation to access in some sections of the study area, the representative orientation of faults were measured in four locations to determine an average fault dip and slip direction to be assigned to faults for which we cannot directly observe the dip or slip direction (Figure 3.4 and Table 1). The orientation of representative faults show steeply dips, striae are sub-vertical and very close to pure normal so we assume that the average slip direction is down dip. Since the representative faults dip both east and west (Figure 3.5), the average will be very steep (87 degrees, Figure 3.6) which may improper for a typical normal fault we found elsewhere in the nature. So we would abandon this average value and will not take it into account in our calculation. We used the average dip of all of the faults, ~74 degrees, instead of the average dip of the average fault which is shown on the stereonet.

The orientation of representative faults and associated striae can be divided into 3 domains with dominate striking of NNW-SSE, east dipping (domain 1), NNE-SSW, west dipping (domain 3) and conjugate mixed set with opposite dips of domain 1 and 3 with the opposite dips and several EW planes (domain 2) (Figure 3.6 and 3.7). The NNW faults (domain 1) are right oblique; 2 slickenlines are left oblique and 4 are right oblique but all are within 15 degrees of pure dip slip. The domain 3 shows NNE west dipping faults as mainly right slip (i.e., a mixture of slightly right and slightly left, very close to pure normal). The mixed set, domain 2, is similarly mixed in their oblique components, so the bottom line is that there really is no strong sense of oblique slip seen in these data and it supports essentially pure normal no matter what the fault orientation.

Table 1. Orientation of a representative faults and slickenlines measured from the field.

Location	Strike/dip	Rake
Loc. #1 10N 0684262 4764166	S83°W 81°W	72°W
	S10°W 80°W	82°SW
	N28°W 89°NE	84°SE
	EW 72°S	89°E
	S53°E 76°S	90°E
	N40°W 63°N	90°S
Loc. #2 10N 0689499 4769354	S32°W 62°W	-
	N18°W 87°NE	81°SE
	S10°W 59°NW	82°SW
	S28°W 54°NW	68°NW
	S11°E 80°W	61°SE
	N29°W 81°NE	76°SE
	N20°W 82°E	74°SE
	S43°E 82°S	78°SE
	N58°W 81°NE	-
Loc. #3 10N 0696718 4768672	N8°E 50°S	-
Loc. #4 10N 0696723 4768656	N44°E 81°SE	55°SW
	N73°E 76°SE	74°E
	N37°W 81°NE	77°N
	N70°E 75°E	74°W
	N33°E 70°E	59°S

Figure 3.4. Location of representative orientation of faults and slickenlines collected from the field. The numbers refer to locations from Table 1.
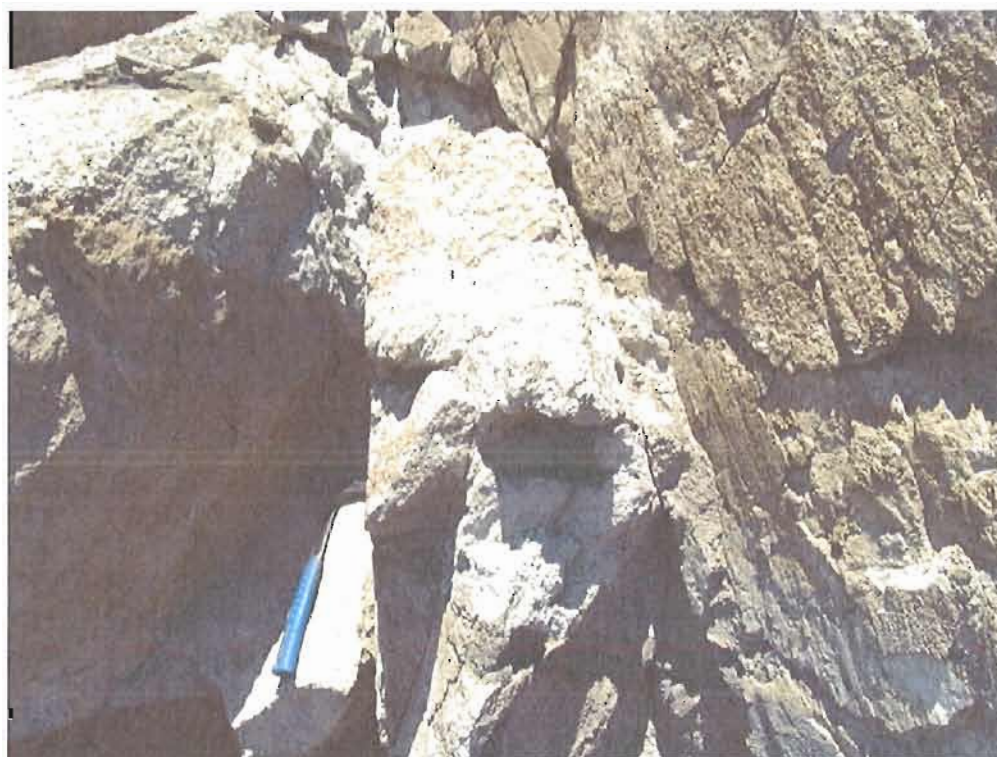
Figure 3.5. The outcrop at location#2 showing faults and associate striae. Faults showing a variety of dips.
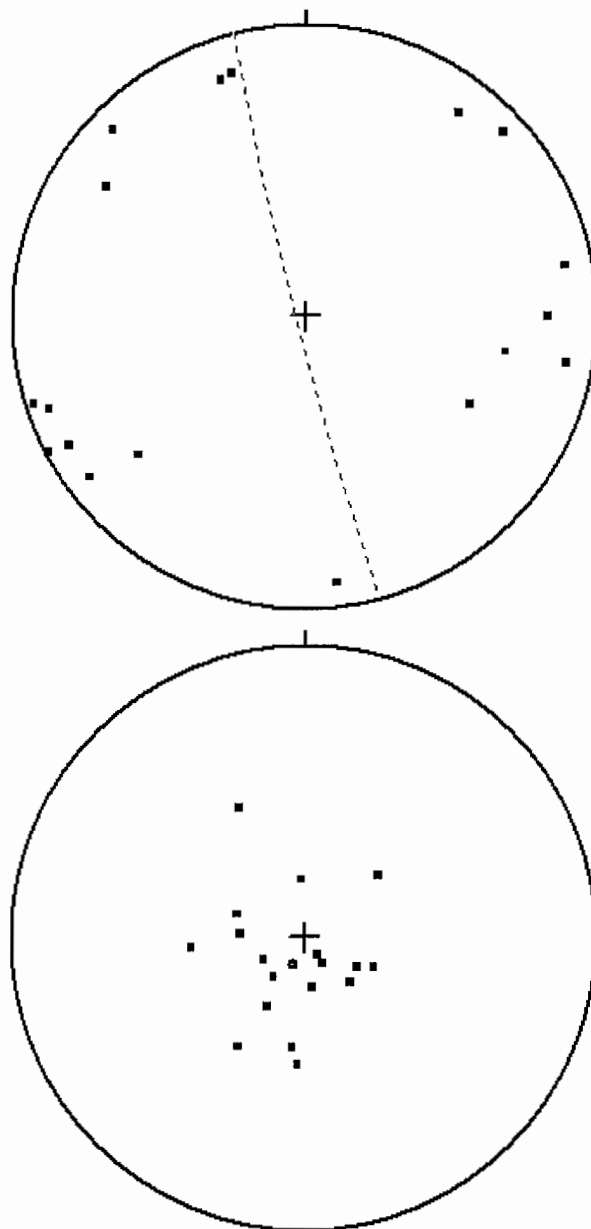
Figure 3.6. Stereonets of representative faults and slickenlines in study area.
(Upper) Poles to fault planes show steep dips regardless of the strike; we used the average dip of all of the faults for our best estimate. Dashed line is the average orientation; because faults dip both east and west, the dip is not meaningful, but the strike, ~N15W, matches our minimum extension direction.
(Lower) Slickenlines on fault planes are steep and suggest generally dip slip motion regardless of the fault strike. Mean lineation direction is 82° S24°W.

Domain 1
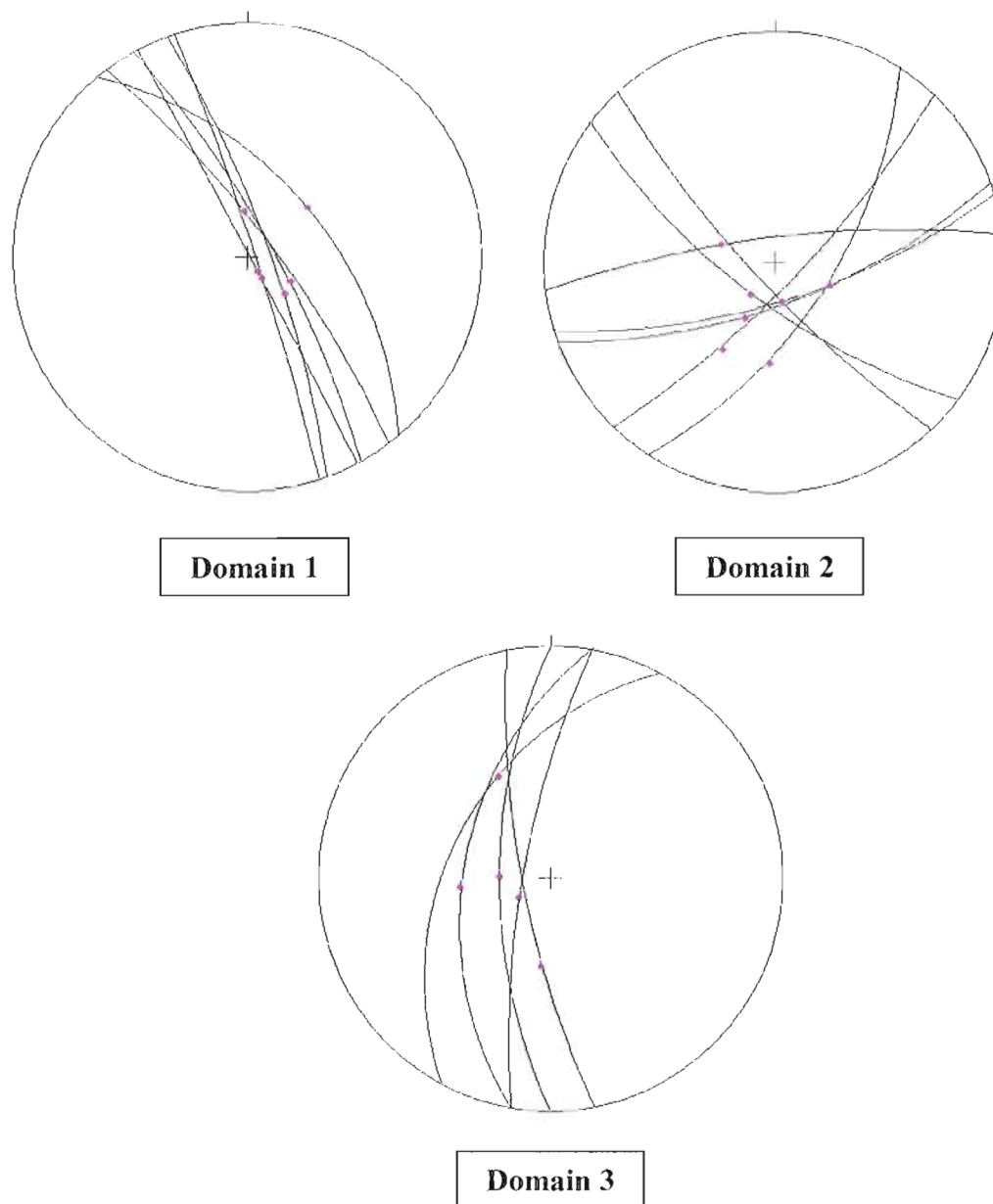
Domain 2

Domain 3

Figure 3.7. Stereonets of faults and slickenlines collected in the field, broken into 3 distinct groups: NNW-SSE, east dipping (domain 1), NNE-SSW, west dipping (domain 3) and conjugate mixed set that included faults with similar trends as domains 1 and 3, but opposite dips, and several EW planes (domain 2).

Extension Direction

As mentioned earlier in Chapter 1, the top-bottom fault traces were broken into 10-meter segments and reference coordinates were assigned to measure the directions and distances in the nearest point analysis (Figure 1.10). The frequencies of offset and extension distribution were plotted azimuthally to see how extension varies with direction. The distribution of the offsets on individual fault was varied by fault geometry regardless of its size. The directional variations of the offset due to faults' geometries are shown in figure 3.8. The straight faults produce little variability (e.g. fault 23) whereas more variable yield a range in both directions (Rose diagram) and offsets (histogram). The straight faults (fault 23) show the dominate NNW trend, bent faults (fault 22) show the two major trends and curved fault provides normal distribution. The peaks of these offset vectors either on histogram or Rose diagram will response to the stretching direction on each fault, combining these directions for all faults will resolve extension direction.

The offsets of every single fault were plotted azimuthally to see the extension direction of the area (Figure 3.9). Azimuthal frequency distribution is bimodal, reflecting the approximately equal number of east and west dipping faults. The fact that the variation changes systematically with azimuth, suggests a single distribution of faults in the study area which probably developed at the same time and their movements were contemporaneous. The maximum extensional direction is ~ N75°E. The fact that extension diminishes to zero at ~N15°W suggests that the minimum horizontal strain axis (and maximum horizontal stress axis) is oriented in this direction. Since there is no
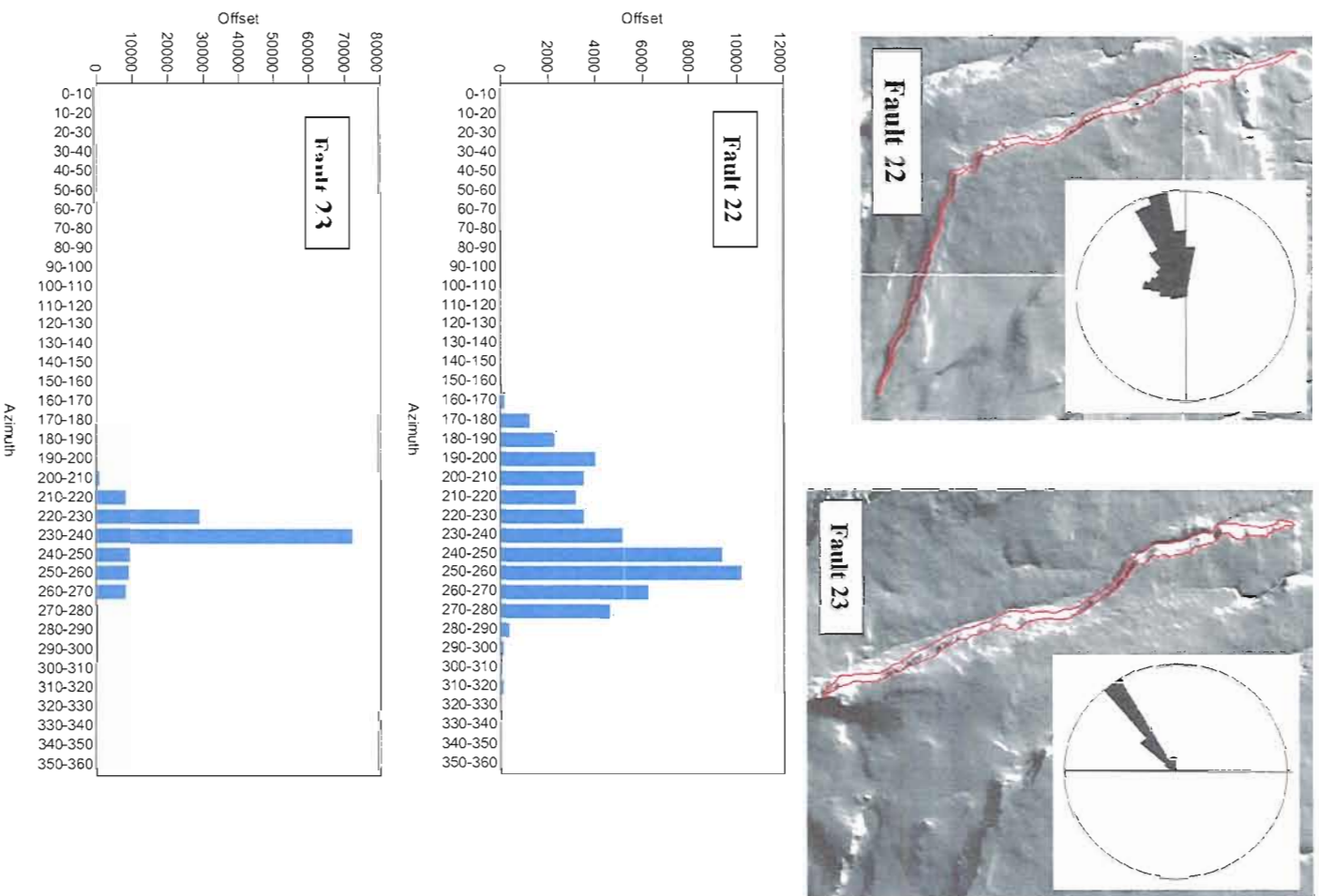
Figure 3.8. The azimuthal variation of the offset for individual fault. Straight fault shows a dominate trend and bent fault shows two dominate trends.

extension in the ~N15°W direction (Figure 3.8), vertical thinning must equal the

extension in the ~ N75°E direction in order to preserve mass. Therefore, this area is

experiencing plane strain. This estimated extension direction is supported by orientation

of faults collected from the field. Representative faults average N15°W direction (Figure

3.5) and if the plane strain assumption is applied, there will be no extension along this

direction.
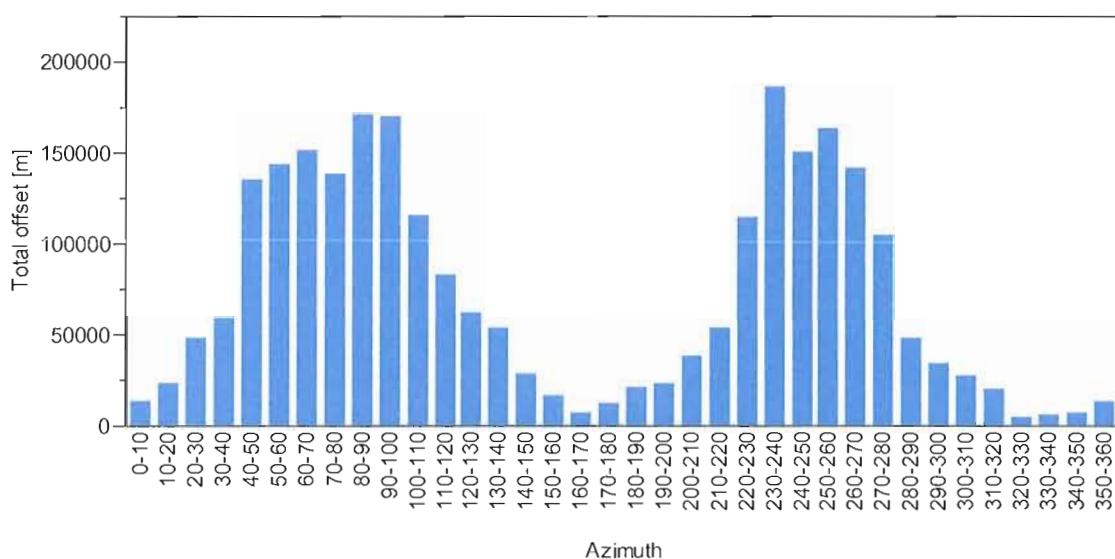
Figure 3.9. Azimuthal distribution of the offset suggesting faults in study area developed at the same time and the movement were contemporaneous

Magnitude of Extension

The top and bottom boundaries of fault scarps were divided into 10-meter

segments where the reference points were generated along the tracing lines. The

coordinates of the reference point on each segment and vertical component displacement

(ΔZ) on top-bottom of each fault were used to calculate the offsets and extension by using the trigonometric relationships

$$\text{offset} = \Delta Z / \text{Sin}(\theta)$$

$$\text{extension} = \Delta Z / \text{Tan}(\theta)$$

where θ is average dip obtained from the field (74.38 degrees in this study). As mentioned in Equation 2 the original area A_o is calculated by measuring the expanded area A_e of the representative area at the north end of Summer Lake basin using GIS and subtracting the area occupied by faults and tilted fault blocks A_a. The length of the major axis has been resolved.

The magnitude of extension is estimated 1.5 to 5.5 percent along the maximum extension direction. Estimated areas added by extension and calculated from equation 1 in Chapter I, are shown in Table 2. The amount of extension is estimated assuming both planar faults to depth and steep surface faults curving into listric detachment fault, providing the minimum and maximum possible extension. The common occurrence of tilted fault surface blocks strongly suggests that faults have curved surfaces rather than planar surfaces at depth (Travis, 1977). The geometry of the main fault in detachment-rooted normal faults can create a void, which is often filled by secondary or antithetic faults. The roll-over structure is specific to a listric fault geometry, while the planar faults provided many antithetic faults (Faure & Chermette, 1989). An array of parallel normal faults associated with minor antithetic faults are commonly observed on the outcrop in the field, suggest that major faults in the study area are listric.

In addition, the average dip measured in the field was much steeper than what most normal faults are believed to have, I also made the calculations assuming 60° degrees and it doubles the amount of extension one would calculate (Table 2).

Tilted Fault Blocks

The blocks between the faults in the study area are nearly flat with the steepest dipping approximately 5 degrees (Travis, 1977). Visually, it appears that the tilt of blocks can be obtained from surface slopes. To make sure that the slope on the surface of the blocks is the dip of beds in the block, the tilt of blocks was measured from the surface slope and compared to the strike and dip determined the from the basalt tracing method described in Chapter 2 (Table 3). Surface slopes generally correspond to the tilt of beds in most places but a few are different. The error may be caused by the discontinuity of bedding planes on fault scraps that make the tracing lines hard to follow. However, results from surface slopes are reasonable and comparable, so we use them where we do not have tilts from the volcanic layering within blocks.

The estimated extension acquired from tilted fault blocks in the study area is consistent with other studies where faults with a dip of 5° to 10° have extension equivalent to about 10% where as faults with dips more than 45° have extension equivalent to more than 100% (Proffett, 1977; Anderson, 1971; Wright & Troxel, 1973). Herein for an average few degrees in the study area indicates 1.5 to 5.5 percent extension. Many studies indicate extension of about 20-30% for entire Great Basin region using a technique that relates dips of bed and extension on the tilted fault blocks (Morton &

Black, 1975) or Proffett (1977) using other data obtained the result that amount of extension in Basin and Range Province varies from area to area. Since our study does not include the major range forming faults (i.e. Winter Rim, Diablo Rim and Abert Rim) we are only seeing a fraction of the total deformation.

Table 2. Estimated strain of the study area.

	Initial dip = 74.38°	Initial dip = 60°
A_e [m^2]	555,369,807.88	555,369,807.88
Planar fault		
A_a [m^2]	7,039,871.59	14,537,708.04
A_o [m^2]	548,329,936.29	540,832,099.84
a-axis	13,211.31	13,120.68
b-axis	13,380.93	13,473.37
Percent change	101.28	102.69
Listric fault		
A_a [m^2]	26,145,643.18	29,075,416.08
A_o [m^2]	529,224,164.70	526,294,391.80
a-axis	12,979.11	12,943.13
b-axis	13,620.33	13,658.18
Percent change	104.94	105.52

Table 3. Comparing amount of tilt obtained from basalt bed and surface slope.

Block ID	Bedding	Measured tilt	
		from bedding plane	from surface slope
2	b2_1	3.350509	2.577035
	b2_2	4.031433	2.577035
4	b4_1	4.259658	4.762176
	b4_2	3.569953	4.762176
	b4_3	7.774043	4.762176
5	b5_1	5.285455	4.91479
	b5_2	9.288711	4.91479
6	b6_1	2.556545	4.729436
	b6_2	5.015185	4.729436
	b6_3	15.399195	4.729436
7	b7_1	5.053379	3.713142
	b7_2	1.860022	3.713142
	b7_3	0.553182	3.713142
	b7_4	2.759043	3.713142
	b7_5	0.955491	3.713142
9	b9	2.953646	1.787224
10	b10	1.101431	2.691441
11	b11	2.682819	2.248956
44	b44	0.386276	0.88942
47	b47	2.280503	2.585157
48	b48	0.440043	1.71695

As discussed above in the Introduction, we initially intended to explicitly include block tilt in our calculations, so we would not have to know the geometry of the faults at depth. However, we found that on average the blocks did not tilt in the extension direction, which makes the calculation of their contribution to extension much more difficult. Thus we decided to simply bracket the extension by assuming the greatest and least possible dips at depth. The fact that the tilt is not in the same direction of its extension, probably means that the dip of low angle faults underneath was not controlled by extension, and thus may have followed pre-existing weakness or regional layering in the volcanic rocks. Result from this study showed blocks tilt on average 60° from the maximum extension direction (Figure 3.10) indicates that the fault pattern in the region was probably controlled by reactivation of basement structure which is approximately N15°E.
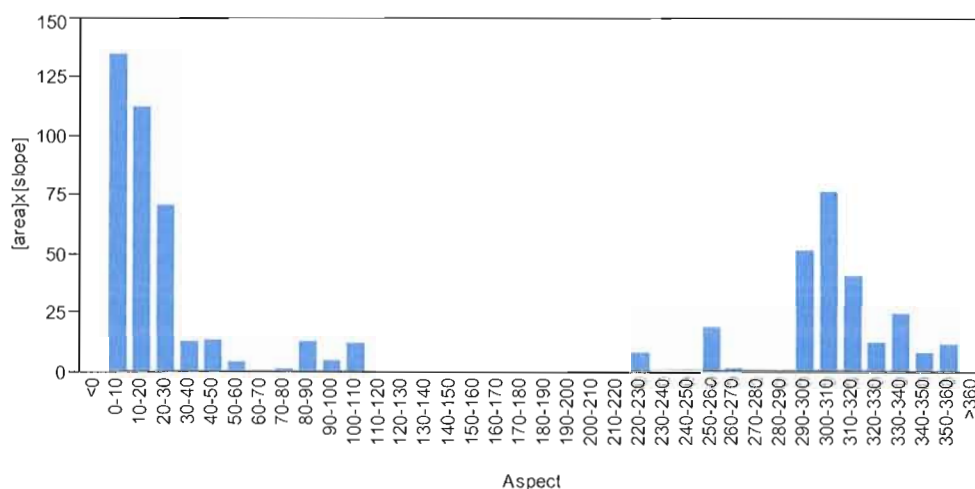

Figure 3.10. Aspect of tilted fault blocks. Blocks tilt on average of 60° from the maximum extension direction (075° and 255°) suggested that the detachment surface is probably controlled by reactivation of basement structure or the pre-existing dip of layering underneath.

We decided not to explicitly use the dips of the blocks because we decided to use the fault displacement to get at extension if the faults are listric (Figure 1.8B). However the tilt of the blocks, and especially the fact that certain regions have consistently dipping blocks suggests that the faults root into some sort of detachment, and thus the approach we use to get the extension that assume a detachment is reasonable. Furthermore, we can fit the strain ellipse to the area added A_a to get the real magnitude and direction of extension (Appendix A). Results indicate total extension of 5.14% in an azimuth of 73.35°, almost identical to the result from GIS technique (Figure 3.11 and 3.12).
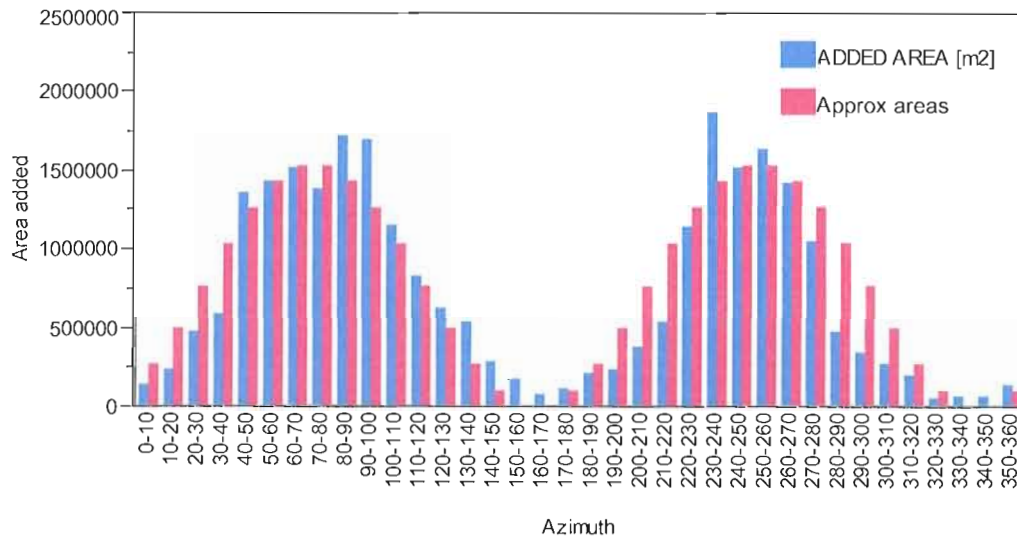

Figure 3.11. Estimated extension using our added area approach compared with an ellipse with the same area. (Red) Added area assuming a perfect strain ellipse. (Blue) Area added from this study.
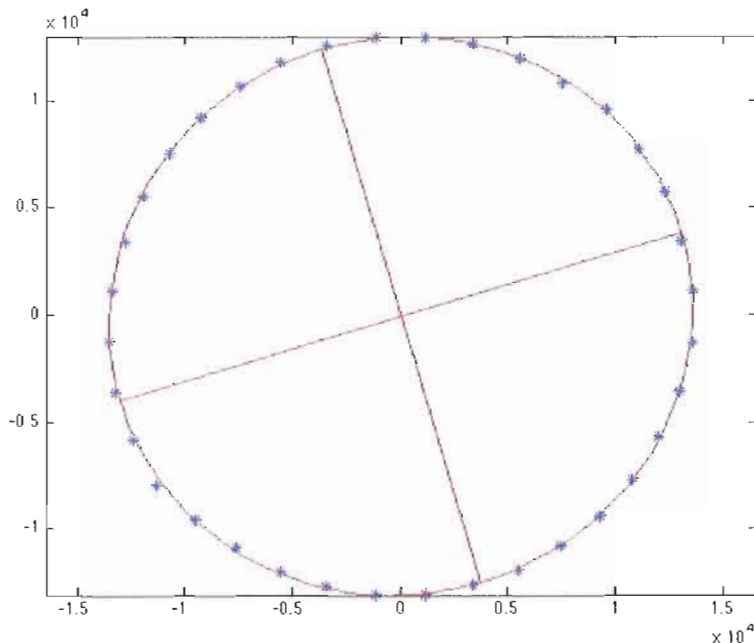
Figure 3.12. Strain ellipse fitting using least squares method. Major axis has a length of 1.0514 and minor axis is rotated 16.6451° West of North indicating extension of 5.14% in the direction of N73°E. The extension data from the GIS technique (blue) very closely matches the shape of the fit ellipse (red).

This new technique does not require one to collect information across the whole region to estimate deformation. Instead, we can pick representative areas that characterize the deformation in a broad area. This method has the advantage for studying areas that are difficult to access and collect data. For instance, Donath (1962) could not determine dips for about 85% of the faults by using air photograph and observations in the field. This new technique provides a methodology to obtain the orientation data and make a robust estimate of the strain. Undoubtedly, this methodology can be applied to any parts of the world especially in other part of Basin and Range Province that undergo uniform deformation, even for some complex regions where we cannot collect the orientation of fault easily such as in the east portion of study area.

APPENDIX A

FITTING AN ELLIPSE TO DETERMINE ADDED AREA

Approximating Radii

In order to determine the size and orientation of a strain ellipse that best matches the azimuthal variation in extension determined from my GIS analysis, I used an ellipse-fitting program written by fellow Graduate Student Sequoia Alba, Because the program requires a list of coordinates (points in *x, y*), I found values for the radius of the ellipse centered between the two outside angles by approximating the area of a 10 degree section of a circle. I then found the radius of that circle for each added area using:

$$ r_e = \sqrt{\frac{(A_e \cdot 36) + A_c}{\pi}} $$

where A_e is the added area in a 10 degree section, A_c = *total expanded area -total added area* (Figure A).The added radius is determined by subtracting the radius of the inscribed circle $d_e = r_e - r_c$. I then used the angles and radiuses to get a list of *x* and *y* coordinates to plug into the ellipse fitting program.

.
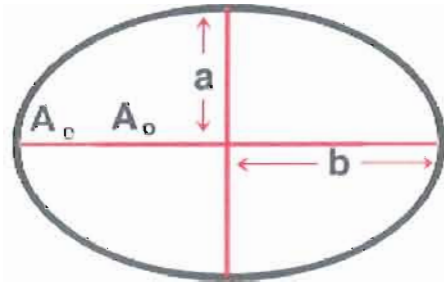
Figure A. Original area in circle A_o and extended area in ellipse A_e. The different area between circle and ellipse is "area added", A_a.

Ellipse Fitting

The ellipse fitting program uses a least squares method to find the equation for the ellipse described by the second order polynomial:

$$Ax^2 + Bxy + Cy^2 + Dx + Ey + F = 0$$

It then finds the "tilt" of the ellipse and subtracts it to get the new equation of the untitled

ellipse: $A'x^2 + C'y^2 + F = 0$. The major and minor axes are inferred from the

coefficients of the polynomial.

Approximated Areas

To get the list of approximated areas I used the parametric equations for an ellipse rotated counter clockwise by ϕ:

$$x = a \cos(\theta)\cos(\phi) - b \sin(\theta)\sin(\phi) \qquad y = a \cos(\theta)\sin(\phi) + b \sin(\theta)\cos(\phi)$$

and integrated the polar equation for the area over 10 degree increments clock-wise from

north: $\int_{\alpha}^{\beta} r^2 d\theta$ with $r^2 = x^2 + y^2$.

The resulting comparison are shown in Chapter 3 (figure 3.11 and 3.12).

APPENDIX B

APPROXIMATED AREAS FROM FITTING ELLIPSE

Azimuth	Added area [m²]	Radii	Approx. areas
0-10	143271.201	63.152	278799.2
10-20	240553.986	105.82	510479.5
20-30	486303.562	212.99	773936.6
30-40	592530.515	259.05	1037394
40-50	1361422.03	587.75	1269074
50-60	1441899.61	621.7	1441033
60-70	1521671.44	655.26	1532531
70-80	1388332.84	599.11	1532531
80-90	1721898.87	739.14	1441033
90-100	1701654.42	730.69	1269074
100-110	1163665.76	503.97	1037394
110-120	832258.647	362.4	773936.6
120-130	631450.321	275.88	510479.5
130-140	540418.387	236.47	278799.2
140-150	288203.757	126.67	106839.8
150-160	176664.459	77.814	15342.11
160-170	80201.968	35.415	15342.11
170-180	125598.525	55.386	106839.8
180-190	222798.243	98.042	278799.2
190-200	237366.259	104.42	510479.5
200-210	390190.258	171.18	773936.6
210-220	544987.117	238.45	1037394
220-230	1148941.99	497.72	1269074
230-240	1870925.84	801.25	1441033
240-250	1515759.05	652.77	1532531
250-260	1646268.96	707.52	1532531
260-270	1422152.01	613.37	1441033
270-280	1052624.87	456.7	1269074
280-290	486268.56	212.97	1037394
290-300	346174.703	151.99	773936.6
300-310	283281.99	124.52	510479.5
310-320	201304.448	88.622	278799.2
320-330	54471.7146	24.083	106839.8
330-340	66516.5467	29.389	15342.11
340-350	73930.3485	32.654	15342.11
350-360	143759.224	63.366	106839.8

Total expanded area: 555369807.88 m²
Total added area: 26145722.4298 m²

REFERENCES

Allison, I. S. (1949). Fault pattern of south-central Oregon [Abstract]. *Geological Society of America Bulletin, 60,* 1935.

Anderson R. E. (1971). Thin skin distension in Tertiary rocks of southeastern Nevada. *Geological Society of America Bulletin, 82,* 43-58.

Badger, T. C., & Watters R. J. (2004). Gigantic seismogenic landslides of Summer Lake basin, south-central Oregon. *Geological Society of America Bulletin, 116,* 687-697.

Clifton, A. E., Schlische, R. W., Withjack, M. O., & Ackermann, R. V. (2000). Influence of rift obliquity on fault-population systematics: results of experimental clay models. *Journal of Structural Geology, 22,* 1491–1509.

Cloos, E. (1955). Experimental analysis of fracture patterns. *Geological Society of America Bulletin, 66,* 241-256.

Cloos, H. (1936). *Einfuhrung in die Geologie.* Berlin: Borntraeger.

Crider, J. G., & Pollard, D. D. (1998). Fault linkage: three-dimensional mechanical interaction between echelon normal faults. *Journal of Geophysical Research, 103,* 24,373-24,391.

Crider, J.G. (2001). Oblique slip and the geometry of normal-fault linkage: mechanics and a case study from the Basin and Range in Oregon. *Journal of Structural Geology, 23,* 1997-2009.

Donath, F.A. (1962). Analysis of Basin and Range structure. *Geological Society of America Bulletin, 71,* 1-15.

Donath, F.A., & Kuo, J.T. (1962). Seismic refraction study of block faulting, South-Central Oregon. *Geological Society of America Bulletin, 73,* 429-434.

ESRI (2007). *Arc GIS 9.2 Help: Near (Analysis).* Retrieved February 6, 2009, from http://webhelp.esri.com/arcgisdesktop/9.2/index.cfm?id=1111&pid=1107&topicname=Near_(Analysis)

Faure, J. L., & Chermette, J. C. (1989). Deformation of tilted blocks, consequences on block geometry and extension measurements. *Bulletin de la Societe Geologique de France, 3,* 461-476.

Hamilton, W., & Myers, W. B. (1966). Cenozoic tectonics of the western United States. *Reviews of Geophysics, 4,* 509-549.

Kautz, S.A., & Sclater, J.G. (1988). Internal deformation in clay models of extension by block faulting. *Tectonics, 7,* 823-832.

Lawrence, R. D. (1976). Strike-slip faulting terminates the Basin and Range province in Oregon. *Geological Society of America Bulletin, 87,* 846–850.

McClay, K. R., & Ellis, P. G. (1987). Analogue models of extensional fault geometries. *Geological Society, London, Special Publications, 28,* 109–125.

Morton, W.H. & Black, R. (1975). Crustal attenuation in Afar. In: Pilger, A. & Rosler, A. (Eds.), *Afar depression of Ethiopia, Inter-Union Commission on Geodynamics Scientific Report No.14* (pp. 55-65). Stuttgart: Schweizerbart.

Pease, R. W. (1969). Normal faulting and lateral shear in northeastern California. *Geological Society of America Bulletin, 80,* 715–720.

Pezzopane, S.K., & Weldon II, R.J. (1993). Tectonic role of active faulting in central Oregon. *Tectonics, 12,* 1140-1169.

Piper, A. M., Robinson, T. W., & Park, C.F., Jr. (1939). Geology and ground-water resources of the Harney basin, Oregon. *U.S. Geological Survey Water-Supply Paper, 841.* 189.

Proffett, J. M., Jr. (1977). Cenozoic geology of the Yerington district, Nevada, and implications for the nature and origin of basin and range faulting. *Geological Society of America Bulletin, 88,* 247-266.

Reches, Z. (1978). Analysis of faulting in three-dimension strain field. *Tectonophysics, 47,* 109-129.

Stewart, J.H. (1980). Regional tilt patterns of late Cenozoic Basin-Range fault blocks, western United States. *Geological Society of America Bulletin, 91,* 460-464.

Travis, P. L., Jr. (1977). *Geology of the area near the north end of Summer Lake, Lake County, Oregon,* Unpublished master's thesis, University of Oregon, Eugene, Oregon.

Weldon, R. J. II., Fletcher, D. K., Weldon, E. M., Scharer, K. M., & McCrory, P.A. (2002). *An update of Quaternary faults of central and eastern Oregon* [CD-ROM]. (U.S. Geological Survey Open-File Report 02-301).

Wright, L. A., & Troxel, B. W. (1973). Shallow-fault interpretation of Basin and Range structure, south-western Great Basin. in DeJong, R., and Scholten, R. (Eds.), *Gravity and tectonics* (pp. 397-407). Amsterdam: Elsevier Scientific Publishing Company.

Zoback, M. L., Anderson, R. E., and Thompson, G. A. (1981). Cenozoic evolution of the state of stress and style of tectonism of the Basin and Range Province of the western United States: Phil. Trans. Roy. Soc. London A, v. 300, 407-434.